$^{40}AR/^{39}AR$ THERMOCHRONOLOGY ACROSS A TRANSECT OF THE EASTERN GRENVILLE FRONT TECTONIC ZONE AND THE WESTERN BRITT DOMAIN OF THE GRENVILLE PROVINCE, GEORGIAN BAY

Steven Grant

Dalhousie University

Department of Earth Sciences
Halifax, Nova Scotia
Canada B3H 3J5
(902) 494-2358
FAX (902) 494-6889

DATE Jan. 12, 1993

AUTHOR Steven L. Grant

TITLE $^{40}Ar/^{39}Ar$ Thermochronology across a Transect of the Eastern Grenville Front Tectonic Zone and the Western Britt Domain of the Grenville Province, Georgian Bay

Degree BSc (Honours) Convocation May Year 1993

Distribution License

DalSpace requires agreement to this non-exclusive distribution license before your item can appear on DalSpace.

NON-EXCLUSIVE DISTRIBUTION LICENSE

You (the author(s) or copyright owner) grant to Dalhousie University the non-exclusive right to reproduce and distribute your submission worldwide in any medium.

You agree that Dalhousie University may, without changing the content, reformat the submission for the purpose of preservation.

You also agree that Dalhousie University may keep more than one copy of this submission for purposes of security, back-up and preservation.

You agree that the submission is your original work, and that you have the right to grant the rights contained in this license. You also agree that your submission does not, to the best of your knowledge, infringe upon anyone's copyright.

If the submission contains material for which you do not hold copyright, you agree that you have obtained the unrestricted permission of the copyright owner to grant Dalhousie University the rights required by this license, and that such third-party owned material is clearly identified and acknowledged within the text or content of the submission.

If the submission is based upon work that has been sponsored or supported by an agency or organization other than Dalhousie University, you assert that you have fulfilled any right of review or other obligations required by such contract or agreement.

Dalhousie University will clearly identify your name(s) as the author(s) or owner(s) of the submission, and will not make any alteration to the content of the files that you have submitted.

If you have questions regarding this license please contact the repository manager at dalspace@dal.ca.

Grant the distribution license by signing and dating below.

_____ _____

Name of signatory Date

ABSTRACT

$^{40}Ar/^{39}Ar$ thermochronology of hornblendes from granitic gneisses and amphibolites in the Central Gneiss Belt (CGB) west of Key Harbour along northern Georgian Bay yields ages ranging from 1016 - 995 Ma. Muscovites from the same area yield ages ranging from 993 - 990 Ma. Hornblendes from two locations in the eastern Grenville Front Tectonic Zone (GFTZ) have similar ages to those found in the CGB; hornblendes sampled further west in the GFTZ portion of the transect have ages ranging from 1120 - 1028 Ma. A single muscovite sample from the western end of the transect is 1112 Ma.

The hornblendes of the CGB and eastern GFTZ are ~35 million years older than hornblendes previously obtained to the southeast in CGB and ~10 million years older than hornblendes previously obtained in the western GFTZ. The ages of the CGB and eastern GFTZ samples seem to be geologically reasonable. The 5 - 11 °C/million years cooling rate of the CGB in the present transect for the 700 - 500 °C temperature range is intermediate between the tectonically-driven, very rapid cooling of the western GFTZ (Haggart 1991) and to the west and the slower rate of ~4 °C/million years in the CGB caused by differential erosion (Check 1989, Culshaw et al. 1991, and Cosca et al. 1991) to the east and south. The ~35 million year difference between the hornblendes in the present transect and hornblendes east of Key Harbour may be the result of extension between 1035 Ma and ~1005 Ma. In this postulated episode of extension, the eastern part of the transect became tectonically denuded following normal faulting with E or SE slip.

Excess argon contaminated the three hornblendes and one muscovite in the western GFTZ, elevating the apparent ages of these samples.

Key words: $^{40}Ar/^{39}Ar$ thermochronology, age spectrum, Central Gneiss Belt, excess argon, exhumation, extension, Georgian Bay, Grenville Front Tectonic Zone, Grenville Province, hornblende, inverse isochron, muscovite, Ontario.

TABLE OF CONTENTS

TABLE OF FIGURES

TABLE OF TABLES

ACKNOWLEDGEMENTS

I would like to thank Dr. Nicholas Culshaw, my advisor, especially for his patience and assistance. His humour in the field helped to make fieldwork enjoyable. My advisor Dr. Peter Reynolds helped greatly by clarifying theoretical aspects of $^{40}Ar/^{39}Ar$ thermochronology and assisting me in interpreting the data. I also appreciate the advice Dr. Barrie Clarke gave on writing and organization. Others who provided valuable input at various stages include: Keith Taylor for assistance in procuring $^{40}Ar/^{39}Ar$ ages, Bob Mackay for setting up the electron microprobe, Gordon Brown for cutting thin sections, and Sandy Grist for instructions and advice on mineral separation procedures. My friends, especially my fellow thesis students of 1991-1992 were very supportive during stressful times, and to them I owe many thanks. I cannot thank my parents enough for their support.

CHAPTER 1: INTRODUCTION

1.1 Application of $^{40}Ar/^{39}Ar$ Thermochronology

The timing of metamorphism and deformation is crucial for an overall understanding of high grade, structurally complex terranes, such as the Grenville province. The radioactive decay of certain isotopes within minerals provides a clock to measure geological time.

This thesis uses the decay of ^{40}K to ^{40}Ar as a clock to determine the age of thermal and tectonic events within the Grenville. The decay of ^{40}K to ^{40}Ar is useful as a geochronological tool for several reasons. Potassium is a widespread element in the crust of the earth and is incorporated into many common minerals. ^{40}K has a very long half-life so it is applicable to dating moderately to very old rocks. Also, various K-rich minerals have different closure temperatures, permitting a determination of the thermal history for a metamorphic terrane.

1.2 Regional Geology

The Grenville Orogeny culminated between 1.15 and 1.00 Ga (Davidson 1985), and the Grenville Province, a structurally complex region which stretches 1900 km from southern Labrador to southwestern Ontario (Fig.1.1, lower

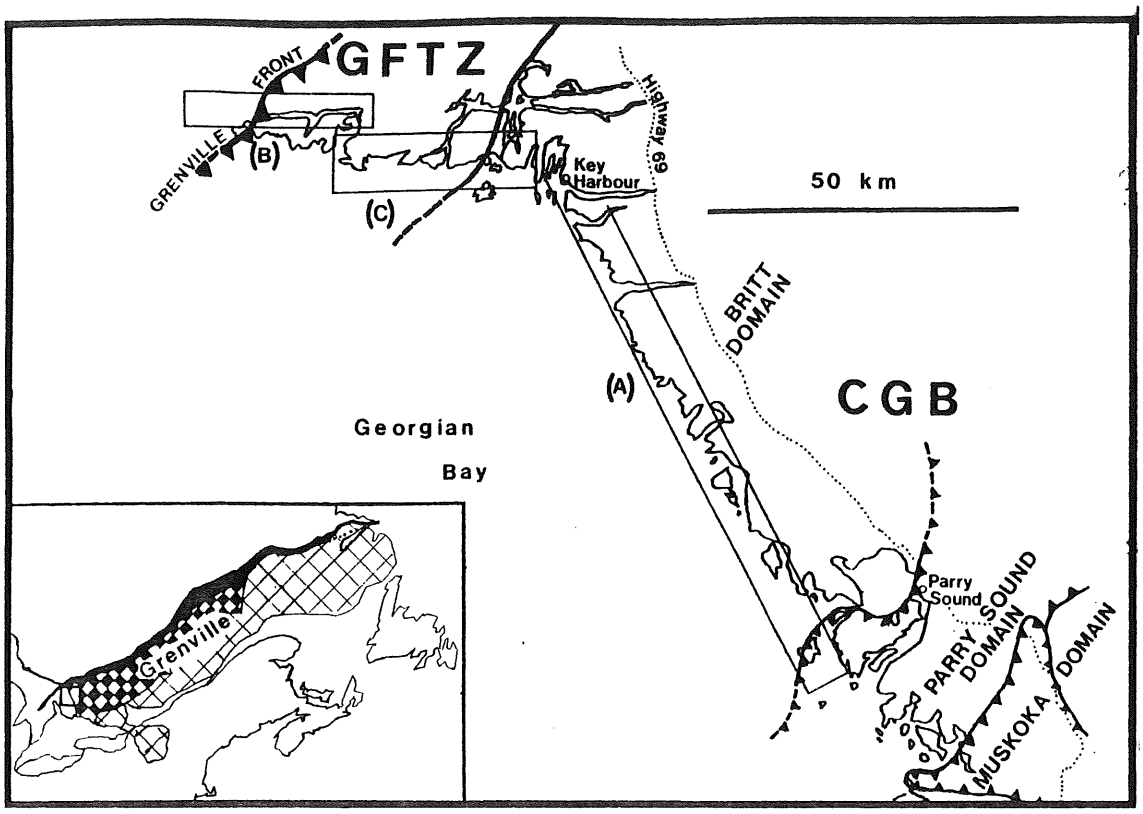

Figure 1. Regional Geology. Inset (lower left): The Grenville Province in relation to eastern North America. The patterned areas represent: the Grenville Front Tectonic Zone (GFTZ), black; the Central Gneiss Belt (CGB), checkerboard; and other regions of the Grenville Province, grid. The small square in the southwestern portion of the Grenville Province is enlarged as the main diagram.

Main Diagram: The Grenville Province exposure on eastern Georgian Bay. The boundary between the Southern Province and the GFTZ is the Grenville Front (heavy toothed line). The thick non-toothed line parallel the Grenville Front represents the southwestern margin of the GFTZ although the GFTZ - CGB transition is gradational. A few of the domains of the CGB along Georgian Bay are shown; they are bounded by shear zones (light toothed lines). The boxed areas represent recent $^{40}Ar\backslash^{39}Ar$ thermochronology studies by Check (1989), Culshaw et al. (1991) and McKenzie (1991), (a); Haggart (1991), (b); and the present study, (c).

left inset) bears the thermal and structural imprint of that orogeny. The present study focuses on the Grenville Front Tectonic Zone (GFTZ) and the Britt Domain of the Central Gneiss Belt (CGB) along Georgian Bay (Fig. 1.1).

In southwestern Ontario, the CGB contains gneisses of both plutonic and supracrustal origin. Within the CGB, anastomosing shear zones define the boundaries of several domains which have been thrust in a northwest direction (Davidson 1984a).

The Grenville Front is the northeast-striking boundary between the generally lower grade, middle to late Proterozoic and Archean rocks to the northwest and the higher grade, more deformed late Proterozoic Grenville Province to the southeast. The Grenville Front is marked by mylonites and ultramylonites, with down-dip lineations and kinematic indicators suggesting that thrust motion was in a northwest direction over the Superior Province (Wynne-Edwards 1972). Gneisses and mylonites parallel to the Front occupy the region between the Grenville Front and the Britt Domain of the CGB. This region, the Grenville Front Tectonic Zone (GFTZ), occupies an approximately 50 km-wide belt along the entire northwestern margin of the Grenville Province (Fig. 1.1, lower left inset). Deformed and metamorphosed equivalents of the Superior Province in the GFTZ (Davidson et al. 1979; Lumbers 1978) indicate that the GFTZ is parautochthonous to the Superior Province.

Granulite and upper amphibolite facies found in much of the exposed surface of the Grenville Province indicate a burial of 20 - 30 km (Davidson 1985), so the Grenville Province may represent the exhumed mid-crustal remains of a mountain belt formed during the Grenville Orogeny. Many of the rocks found within the Grenville Province have their origins as Archean foreland or as Proterozoic accreted terranes (Nunn et al. 1990; Gariépy et al. 1990; Dickin and McNutt 1989) but the rocks of the Grenville Province generally bear a characteristic 1.15 - 1.00 Ga metamorphic and tectonic overprint (Davidson 1985).

1.3 Purpose

1.3.1 Significance

Studies of complex Precambrian orogens like the Grenville help reveal the mechanics of crustal accretion and mountain-building. The Grenville Orogen is informative because the exposed rocks were formed at deep orogenic levels; the exposed structures and metamorphic assemblages may provide an understanding of mid-crustal processes.

1.3.2 Previous thermochronology

Previous $^{40}Ar/^{39}Ar$ studies by Check (1989), McKenzie (1991), and Culshaw (1991) in the Britt and Parry Sound domains (Fig. 1.1) show a general increase in age from south to north for mica and K-feldspar. Higher cooling rates in

the north or an elevated geotherm in the south could account for this trend. The average of hornblende ages in a transect of the Britt Domain (Culshaw et al. 1991) is ~970 Ma. The difference between hornblende ages and muscovite ages is approximately 70 million years.

Haggart (1991) records $^{40}Ar/^{39}Ar$ ages of 996 ± 5 Ma, 994 ± 5 Ma, and 979 ± 9 Ma for three hornblendes in the eastern part her study area within the GFTZ along Georgian Bay; hornblende ages become higher and less consistent approaching the Grenville Front to the northwest. Igneous and metamorphic titanites sampled from across the GFTZ define a single discordia with an upper intercept of 1446 +10/-11 Ma and a lower intercept of 985 +21/-20 Ma. Generally, the degree of discordance (distance away from the upper intercept along the discordia) corresponds to the geological distance from the Grenville Front, so that the titanite farthest away from the Grenville Front (adjacent to the present thesis area) is the closest to being completely reset at ~985 Ma. Her interpretation is that the thermal pulse had decreasingly lesser effects toward the Grenville Front (away from the 'core' of the orogen). Because the titanite and hornblendes in the southeastern portion of her study area record the same ~985 Ma event, yet titanite and hornblende reset at different temperatures, Haggart (1991) concluded that the exhumation must have been very rapid.

There are several important differences between the results of Haggart (1991) in the GFTZ and Check (1989), Culshaw et al. (1991) and McKenzie (1991) in the CGB. The hornblende ages in the CGB are relatively consistent at ~970 Ma, while the 996-979 Ma hornblende ages at the eastern edge of the area studied by Haggart (1990) increase westward. Cooling from the closure temperature of titanite to the closure temperature of hornblende and potassium feldspar appears almost instantaneous at the eastern end of the area studied by Haggart (1991), while cooling from the closure temperature of titanite to the closure temperature of hornblende required ~70 million years in the CGB.

Excess argon is a problem in the Grenville Province; for instance, biotites to the east in the Britt Domain (Check 1989) and to the west in the GFTZ (Haggart 1991), give unreliable ages because of excess argon contamination, although hornblendes and muscovites seem to be unaffected. Easton (1986) discusses excess argon in biotites near the Grenville Front. Although biotites are more likely to incorporate excess argon than muscovites (Roddick et al. 1980) and biotites near the present transect contain excess argon (Check 1989, Culshaw et al. 1991, and Haggart 1991), other minerals are also susceptible to excess argon contamination. The documentation of excess argon in the northern Georgian Bay area indicates that all $^{40}Ar/^{39}Ar$ thermochronological studies in the area should proceed with caution.

1.3.3 Objectives

This thesis derives $^{40}Ar/^{39}Ar$ age dates for hornblendes and muscovites on a transect along Georgian Bay (Fig 1.1) The objectives of this undertaking are:

1) Determine $^{40}Ar/^{39}Ar$ ages for hornblende and muscovite in the ~50 km gap between the area studied by Check (1989); Culshaw et al. (1991) and the area studied by Haggart (1991).

2) Compare geochemistry determined from microprobe analysis of hornblende with geochemistry determined from isotope data collected during $^{40}Ar/^{39}Ar$ analysis of hornblende. The microprobe information acts as an independent test of sample purity and suitability.

3) Determine if the trend of increasing muscovite ages to the north continues into the present study transect.

4) Determine the nature of the transition of the ~970 Ma hornblende ages east of Key Harbour in the Britt Domain to the 985 Ma hornblende ages west of Beaverstone Bay in the GFTZ.

5) Use the thermochronology information to determine the thermal history of the area, and then construct a possible tectonic interpretation.

1.4 Organization

Chapter 1 introduces $^{40}Ar/^{39}Ar$ thermochronology, the regional geology, previous work in the region, the objectives of the thesis and the study area. Chapter 2 discusses the theory behind $^{40}Ar/^{39}Ar$ thermochronology, including explanations of K-Ar decay, closure temperature, age spectra interpretation and inverse isochrons. Sample descriptions, sample preparation and sample analysis are discussed in Chapter 3. The results of the $^{40}Ar/^{39}Ar$ analysis and the hornblende microprobe study are presented and discussed in Chapter 4. Chapter 5 outlines the thermal and tectonic interpretations and Chapter 6 presents the major conclusions.

1.5 Introduction to the Transect

The ~50 km transect on the northern shore of Georgian Bay stretches from the eastern side of Beaverstone Bay to the mainland north of Dead Island (Fig. 1.2). Along this shore, the GFTZ and Britt Domain form nearly continuous outcrop easily accessible by boat. Boat launching facilities near Highway 69 provide access to Key River. Key Harbour is 13 km westward along Key River from the highway.

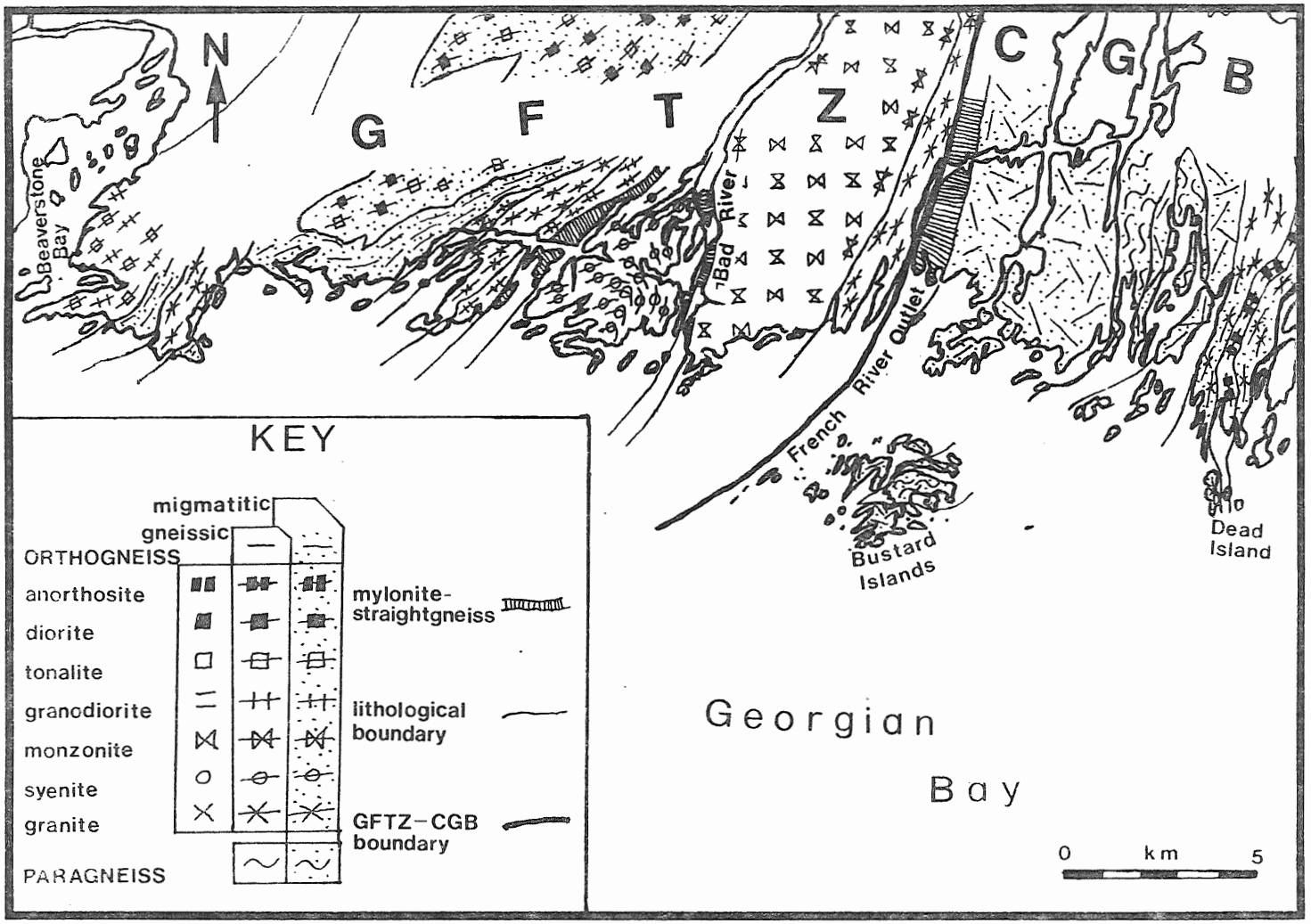

Figure 1.2. Geology of the transect. After Davidson and Bethune (1988).

From the western edge of the transect at Beaverstone Bay to the eastern boundary of the GFTZ at the Main Outlet of the French River, northwest-striking orthogneisses and mylonites, some migmatitic, form a complicated and highly deformed terrane (Davidson and Bethune 1988). The rocks are of varied plutonic origin, and units range in size from a few centimetres to a few hundred meters in width. In some locations the orthogneisses wrap around fairly undeformed plutonic "lumps" (Davidson and Bethune 1988).

Davidson et al. (1982) used strongly foliated orthogneisses and annealed mylonites at the Main Outlet of the French River to define the eastern boundary of the GFTZ. Large-scale folds to the east of this transect in the Britt domain have near subhorizontal south-southeast-plunging axes in most of the Britt domain (Davidson and Bethune 1988; Culshaw et al. 1988). Towards the western edge of the Britt domain, however, structures become parallel with the GFTZ, and the lineation plunges more steeply to the southeast (Davidson et al. 1982). Metasedimentary gneisses and orthogneisses are both common in the Britt Domain (Davidson and Bethune 1988).

CHAPTER 2: $^{40}Ar/^{39}Ar$ THEORY

2.1 Introduction to the ^{40}K-^{40}Ar Decay Series

2.1.1 Potassium decay

Potassium, the eighth most abundant element in the earth's crust, has three naturally occurring isotopes: ^{39}K (93.26%), ^{40}K (.01%), and ^{41}K (6.73%) (Bowen 1988). ^{40}K is radioactive and undergoes branching decay; 89% of a given amount of the ^{40}K undergoes β-emission to produce ^{40}Ca, while 11% breaks down by κ-capture, producing stable ^{40}Ar. ^{40}Ca is the most abundant naturally occurring isotope of calcium, so the small amount produced by the radioactive decay of ^{40}K is virtually undetectable (Bowen 1988). Argon, on the other hand, is not normally incorporated into minerals when they form. Moreover, ^{40}K is the only naturally occurring isotope which breaks down to ^{40}Ar, so the ^{40}K-^{40}Ar decay process is useful as a geochronological tool.

2.1.2 K-Ar age determination

As the decay process progresses, less ^{40}K remains while the amount of daughter ^{40}Ar isotope increases. The decay of ^{40}K occurs at a constant rate which is not affected by geological or physical processes (Bowen 1988), thus the amount of ^{40}Ar relates to the amount of ^{40}K by the following expression:

$$^{40}Ar^{*} = {}^{40}Ar_{i} + (\lambda_{\kappa}/\lambda)(^{40}K)(e^{\lambda t}-1) \qquad \text{(Eqn. 2.1)}$$

where:

$^{40}Ar^{*}$ = the amount of radiogenic ^{40}Ar produced from ^{40}K

$^{40}Ar_{i}$ = the amount of ^{40}Ar from other sources,

λ = the total decay constant for the breakdown of ^{40}K (5.543×10^{-10} year^{-1}),

λ_{κ} = the decay constant for the κ-capture reaction of ^{40}K ($.581 \times 10^{-10}$ year^{-1}), and

t = the time since radioactive decay began within a closed system.

Note that $^{40}Ar^{*}$ refers to ^{40}Ar derived from the breakdown of ^{40}K within the same mineral, a convention followed in the rest of Chapter 2 to distinguish it from ^{40}Ar of other sources. Generally, $^{40}Ar_{i} = 0$ (Bowen 1988), so Equation 2.1, rearranged to solve for t, appears as:

$$t = 1/\lambda \ \ln[(^{40}Ar^{*}/^{40}K)(\lambda/\lambda_{\kappa})+1] \qquad \text{(Eqn. 2.2)}$$

Equation 2.2 is the basis of K-Ar dating. Determining the age of a K-bearing mineral requires a measurement of the ratio of ^{40}K to $^{40}Ar^{*}$. Because $^{40}Ar^{*}$ and ^{40}K require different measurement procedures, two aliquots are necessary. Methods for measuring K include flame photometry, atomic absorption, and X-ray fluorescence (McDougall and Harrison 1988). Measuring $^{40}Ar^{*}$ involves degassing a K-bearing mineral <u>in-vacuo</u> and analyzing the gas on a mass-spectrometer.

For the $^{40}Ar/^{40}K$ ratio to produce a geologically significant age, several assumptions must be met.

1) the rate of ^{40}K decay is constant,

2) the isotopic composition of K is constant,

3) all ^{40}Ar measured is the product of ^{40}K decay (no excess ^{40}Ar from other sources), and

4) no ^{40}Ar has escaped from the sample since the system first closed.

McDougall and Harrison (1988) believe that assumptions 1) and 2) are generally valid. However, the extraction furnace may produce ^{40}Ar while heating the sample. Geological events may cause a mineral to lose accumulated $^{40}Ar^{*}$ or to trap ^{40}Ar from surrounding fluids. The K-Ar method has little potential to make corrections for these problems, so recently the $^{40}Ar/^{39}Ar$ technique has received more attention.

2.1.3 $^{40}Ar^{*}/^{39}Ar$ technique

Merrihue and Turner (1966) pioneered the $^{40}Ar^{*}/^{39}Ar$ technique. Because potassium-bearing minerals contain ^{39}K and ^{40}K today in a constant ratio, a measurement of ^{39}K indirectly measures ^{40}K. Measuring ^{39}K provides no advantage over measuring ^{40}K, but neutron bombardment can convert a portion of ^{39}K to ^{39}Ar at a determinable rate; the amount of ^{39}Ar is thus proportional to the amount of ^{40}K (McDougall and Harrison 1988). Equation 2.3 (Mitchell 1968) represents the conversion process:

$$^{39}Ar = (^{39}K)(\Delta T)\int \phi(\epsilon)\sigma(\epsilon)\, d\epsilon \qquad \text{(Eqn. 2.3)}$$

where:

ΔT = irradiation time,
$\phi(\epsilon)$ = the neutron flux density at energy ϵ, and
$\sigma(\epsilon)$ = the capture cross-section of the ^{39}K for neutrons possessing energy ϵ.

Equation 2.1 combined with Equation 2.3 makes an expression for the $^{40}Ar^*/^{39}Ar$ ratio:

$$^{40}Ar^*/^{39}Ar = \frac{(\lambda_\kappa/\lambda)(^{40}K/^{39}K)(e^{\lambda t}-1)}{(\Delta T)\int \phi(\epsilon)\sigma(\epsilon)\ d\epsilon} \qquad \text{(Eqn. 2.4)}$$

The parameters $\phi(\epsilon)$ and $\sigma(\epsilon)$ are difficult to determine practically, so Grasty and Mitchell (1968) and Mitchell (1966) devised a parameter, J, to replace a part of the expression in Equation 2.4:

$$J = (\lambda/\lambda_\kappa)(^{39}K/^{40}Ar^*)(\Delta T)\int \phi(\epsilon)\sigma(\epsilon)\ d(\epsilon) \qquad \text{(Eqn. 2.5)}$$

where J roughly represents the efficiency of conversion of ^{39}K to ^{39}Ar. Substituting Equation 2.5 into Equation 2.4 produces a simplified expression:

$$^{40}Ar^*/^{39}Ar = (e^{\lambda t}-1)/J. \qquad \text{(Eqn. 2.6)}$$

Rearranged to solve for t, Equation 2.6 becomes:

$$t = (1/\lambda)\ \ln[(^{40}Ar^*/^{39}Ar)(J)+1]. \qquad \text{(Eqn. 2.7)}$$

In practice, the measurement of the parameter J involves the inclusion of a K-bearing mineral of known age (called a flux monitor) with the experimental samples of unknown age during irradiation in the reactor (Merrihue and Turner 1966). Entering the $^{40}Ar^*/^{39}Ar$ ratio of the flux monitor into the following modification of Equation 2.6 yields the J-value:

$$J = \frac{e^{(\lambda t_{fm})-1)}}{(^{40}Ar^*/^{39}Ar)_{fm}} \qquad \text{(Eqn. 2.8)}$$

where:

t_{fm} = the age of the flux monitor (known) and

$(^{40}Ar/^{39}Ar)_{fm}$ = the isotope ratio of the flux monitor (measured).

The age of the experimental samples (t) can be calculated by Equation 2.7 using the substitution of J from Equation 2.8. Dalrymple and Lanphere (1981) determined the following expression to calculate the error in (t):

$$\sigma_t^2 = \frac{(J)^2(\sigma_F)^2 + (F)^2(\sigma_J)^2}{(\lambda)^2[1 + (F)(J)]^2} \qquad \text{(Eqn. 2.9)}$$

where:

σ_t = the standard deviation in t,
σ_J = the standard deviation in J,
F = $^{40}Ar^*/^{39}Ar$, and
σ_F = the standard deviation in $^{40}Ar^*/^{39}Ar$.

Besides converting ^{39}K to ^{39}Ar, the irradiation process also produces ^{36}Ar, ^{37}Ar, ^{38}Ar, ^{39}Ar and ^{40}Ar from isotopes of Ca, K, and Ar. While these interfering isotopes could potentially introduce error into the measurement of Ar ratios, correction factors, determined at each reactor facility, can minimize their effect (McDougall and Harrison 1988).

The $^{40}Ar^*/^{39}Ar$ technique has several advantages over the K-Ar method. The K-Ar method requires different equipment to measure ^{40}Ar and ^{40}K, thus a sample must be divided into two aliquots with great care. Absolute measurements of the total amount of ^{40}Ar and ^{40}K are necessary. $^{40}Ar^*/^{39}Ar$ dating requires only the $^{40}Ar^*/^{39}Ar$ ratio; ratios are easier to

measure than absolute amounts. The most important advantage of the $^{40}Ar^*/^{39}Ar$ method is that the $^{40}Ar^*/^{39}Ar$ ratio, measured on only one machine, can be determined at different temperature increments during a procedure known as step-heating (Hanes 1991).

The $^{40}Ar^*/^{39}Ar$ ratio can vary depending on the depth within the crystal and the type of lattice site. Since a K-Ar sample analysis measures all of the ^{40}K and all of the $^{40}Ar^*$ at one time it will homogenize the ratio. Step heating does not homogenize the ratio; incremental step heating can reveal patterns of $^{40}Ar^*/^{39}Ar$ ratio variation.

2.2 Closure Temperature

The rate of $^{40}Ar^*$ production should be equal throughout the crystal, assuming homogeneous distribution of the parent ^{40}K throughout the crystal lattice. Diffusion depends on temperature, the radius of the mineral through which ^{40}Ar must travel, grain shape, and cooling rate. When the temperature of a rock is very high, ^{40}Ar diffuses rapidly out of all crystal sites and does not accumulate, as shown by the horizontal segment on the bottom graph of Figure 2.1.

The cooling mineral reaches a temperature range at which the diminishing diffusion rate cannot keep pace with the steady $^{40}Ar^*$ production rate, so the mineral partially retains $^{40}Ar^*$ (Dodson 1973). As cooling proceeds, the rate of

argon accumulation increases. The concave upwards portion of the bottom graph on Figure 2.1 represents this regime of partial $^{40}Ar^*$ retention.

When the cooling mineral reaches a temperature at which all $^{40}Ar^*$ diffusion ceases, $^{40}Ar^*$ retention from then on is complete, so the lower graph in Figure 2.1 records a linear increasing trend for $^{40}Ar^*$ accumulation. The apparent age is calculated by extrapolating the linear portion of the $^{40}Ar^*$ accumulation curve through the t-intercept. The temperature (Fig. 2.1, top graph) which corresponds to apparent age is the closure temperature (T_c), (Dodson 1973) (Fig. 2.1).

Dodson (1973) derived an equation which calculates the closure temperature of minerals by iteration:

$$T_c = \frac{E/R}{\ln\left[\frac{(A)(R)(T_c^1)^2(D_o/a^2)}{(E)(dT/dt)}\right]} \qquad \text{(Eqn.2.10)}$$

where:

T_c = closure temperature,
E = calculated activation energy,
R = gas constant (1.987 cal/mol °K),
A = diffusion geometry,
dT/dt = cooling rate,
D_o = diffusion frequency factor,
a = effective diffusion distance of the grain, and
T_c^1 = first approximation of the closure temperature.

Note that T_c occurs on both the right and left side of Equation 2.10. A rough estimate of the closure temperature, entered as T_c^1, gives a better approximation of T_c, which can be re-entered as T_c^1. A continuation of this process

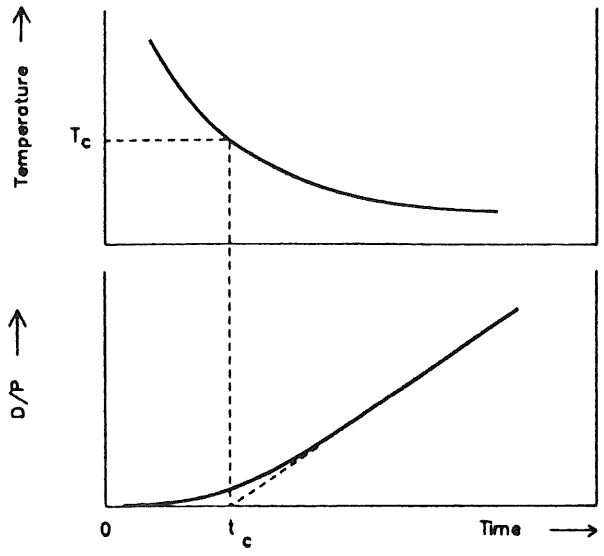

Fig. 2.1. Closure model. The lower graph displays the daughter/parent ratio(D/P) on the y-axis against time on the x-axis. The graph of D/P verses t is horizontal when the temperature, T, is high (top graph) because all daughter product, $^{40}Ar^*$, diffuses out of the crystal. The D/P verses t graph forms a concave upward shape as the temperature decreases because the mineral partially retains $^{40}Ar^*$. When diffusion effectively ceases, the graph displays a linear trend representing total $^{40}Ar^*$ accumulation. Extrapolation of the linear portion of the graph to the time line yields the time of closure, t_c, and thus, the temperature of the closure (upper graph). (from Dodson 1973).

Mineral	Temperature range
Hornblende	450-550 °C
Muscovite	300-400 °C

Table 2.1. Estimated ranges of the closure temperatures of hornblende and muscovite (from Hanes 1991).

eventually yields the unique closure temperature (i.e. $T_c^1 = T_c$).

If precisely controlled, the heating time and temperature data obtained while deriving an $^{40}Ar/^{39}Ar$ age can also provide parameters for Equation 2.10 (Hanes 1991). This is accomplished by plotting the data as an Arrhenius plot of $\log(D/a^2)$ versus (1000/T). The slope and $\log(D/a^2)$ axis intercept yield the parameters E/R and (D_o/a^2) respectively, which are necessary for Equation 2.10.

The diffusion data only have meaning for anhydrous minerals such as feldspars, which remain stable throughout the entire degassing experiment. Hydrous minerals such as hornblende and muscovite break down by dehydration reactions during step heating. For instance, Lee et al. (1991) show that their hornblende sample developed irreversible physical changes (Lee et al. 1991, p. 874) above 930 °C. Temperatures above 1050 °C resulted in the breakdown of hornblende into ilmenite, titanomagnetite, glass, pyribole, residual amphibole, and voids (Lee et al. 1991, p.874). At 1130 °C, the products melted. For the hornblendes from the study of Lee et al. (1991) and from the present study in the Grenville, 930 °C and 1050 °C correspond to the earliest stages of substantial degassing. Clearly the data obtained from even higher temperatures will not represent $^{40}Ar^*$ diffusion out of hornblende, so diffusion experiments for hornblendes are not appropriate.

Hanes (1991) compiled estimates of closure temperatures for hornblendes and muscovites (Table 2.1) which will be adopted for interpretation in this thesis.

2.3 Age Spectra and their Interpretation

2.3.1 Introduction

Step heating allows the calculation of a separate age for each portion of the gas. The standard means of presenting the data is on a plot called an age spectrum (Turner et al. 1966), where the y-axis represents the sample age and the x-axis represents the percentage of the ^{39}Ar released, which cumulatively increases with temperature (Fig. 2.2). The horizontal length of each bar displays the percentage of gas released in each heating step, while the vertical thickness of each bar corresponds to the range of error in the age.

What do age spectra represent? At low heating temperatures, the $^{40}Ar^*$ held loosely by the crystal lattice degasses. $^{40}Ar^*$ held more tightly in lattice sites requires a higher temperature to diffuse out of the lattice. Turner et al. (1966) used simple volume diffusion to explain age spectral patterns; "loosely held" $^{40}Ar^*$ represents $^{40}Ar^*$ which only has to diffuse from the margin of a crystal, while "tightly held" $^{40}Ar^*$ must diffuse from the interior to the surface of the crystal. On the horizontal axis of the age

spectrum, the lowest values of ^{39}Ar released correspond to the gas released by the crystal margin. The gas is sampled from progressively deeper in the crystal as the percentage ^{39}Ar released increases. A discussion of the problems with this interpretation follows in Section 2.4.5.

The total gas age (TGA) is a weighted average of ages from all heating increments. If the ages are similar for all the heating steps, calculating a TGA is appropriate. Often, however, analysis show systematic changes of age with gas release. If this is the case, the pattern revealed by the disparity of ages in the age spectrum can be more valuable as an interpretive aid than the TGA.

2.3.2 Plateau ages

Often the first gas and the last gas evolved from a step heating analysis have anomalously high or low ages, leaving the central portion of the spectrum relatively flat (i.e. of one age). The flat portion represents a plateau age (Fig. 2.2). In practice the plateau age represents the age of mineral closure, providing the plateau is not an artifact of gas homogenization or the gas from each step does not contain excess argon.

Fleck et al. (1977) suggested that a plateau must consist of contiguous steps which have the same age within 95% confidence and comprise at least 50% of the ^{39}Ar released. Equation 2.11 permits calculation of the critical

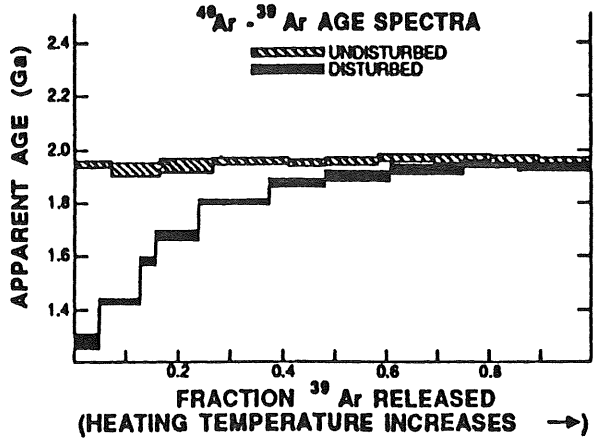

Fig. 2.2. Idealized $^{40}Ar/^{39}Ar$ spectra. The top hatched graph displays an undisturbed spectrum or plateau, while the bottom solid graph displays a disturbed spectrum. Each "block" within the spectrum represents the analysis of the gas from one heating increment. See text for further description. From Hanes (1991).

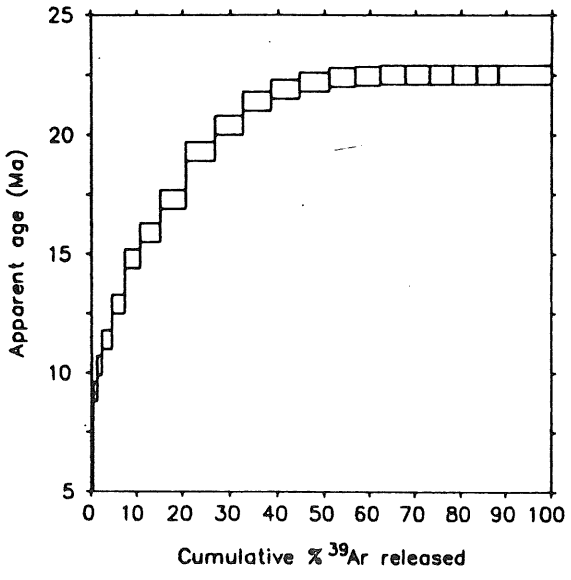

Fig. 2.3. Theoretical spectra for slow cooling minerals. See text for description. From McDougall and Harrison (1988).

value (c.v.) which assesses the agreement of ages between any two steps (Dalrymple and Lanphere 1969).

$$c.v. = 1.960(\sigma_1^2 + \sigma_2^2)^{1/2} \qquad \text{(Eqn. 2.11)}$$

The parameters σ_1 and σ_2 are the standard deviations of the two steps tested. In order for any two steps to be within 95% agreement, the difference between their ages must be less than the critical value calculated for those two steps (Dalrymple and Lanphere 1969).

2.3.3 ^{39}Ar recoil

Besides converting ^{39}K into ^{39}Ar, the bombardment of the sample with energetic neutrons may also cause ^{39}Ar recoil. In this effect, a fast neutron collides with a ^{39}K nucleus, displacing it by as much as 0.5μm from its lattice site. The reduction in the amount of ^{39}Ar causes a higher $^{40}Ar/^{39}Ar$ ratio measurement and thus a higher apparent age. ^{39}Ar recoil normally affects the outer edge of crystals, producing a sharp peak in age for the first gas released.

2.4 Disturbed Spectra and their Interpretation

2.4.1 Introduction

Plateaux which meet the criteria of Fleck et al. (1977) represent one age - the age of mineral closure. In most spectra the plateau does not include all steps, and many

spectra have no plateau at all. Spectra in which a large proportion of the steps vary greatly in age are called disturbed spectra (Fig. 2.2).

2.4.2 Slow cooling diffusivity

A cooling rock can reach a temperature range in which the mineral partially retains $^{40}Ar^*$ (Section 2.2). If volume diffusion is the mechanism of $^{40}Ar^*$ loss, then the outer crystal portions lose $^{40}Ar^*$ more quickly than the core because the $^{40}Ar^*$ in the core must travel a greater distance to reach the crystal surface. In a quickly cooling mineral, volume diffusion has no time to affect the $^{40}Ar^*$ distribution within the lattice, thus all lattice sites within the crystal will have essentially the same age. For slowly cooling rocks, however, the relatively long time spent in the partial retention regime causes the outer portions of the mineral to lose more $^{40}Ar^*$ than the core.

A spectrum for a slow cooling event, as in Figure 2.3, should display increasing ages for the first gas released which level off to a plateau for the later portions of gas released (McDougall and Harrison 1988). This distribution reflects the fact that the core began to accumulate $^{40}Ar^*$ before the margin.

2.4.3 Short-lived thermal event

A thermal event affecting a mineral previously cooled below its closure temperature will reactivate $^{40}Ar^*$ diffusion. If the episode is short-lived, the outer margin

of the crystal will lose more $^{40}Ar^*$ than ^{40}K decay produces but the inner crystal will not lose any at all. As the duration of the thermal event increases, so does the depth to which the $^{40}Ar^*/^{39}Ar$ clock resets (Turner et al. 1966).

The spectrum for a short-lived thermal event (Fig. 2.4) shows the first gas released as a convex upward curve which flattens to a plateau with increasing ^{39}Ar release. The first increment of gas theoretically represents the age when the thermal disturbance ended. The plateau represents the unaffected core. If the thermal event was longer even the core would undergo $^{40}Ar^*$ loss, thus reducing the length of the plateau. While such a spectrum is potentially very useful, McDougall and Harrison (1988) point out that the spectrum shape bears a close resemblance to the spectra of slow cooled minerals (Fig. 2.3 and Fig. 2.4).

2.4.4 Excess argon

As a mineral forms it may incorporate argon from its surroundings, adding ^{40}Ar from a source external to its own reservoir of $^{40}Ar^*$. If the trapped argon has an atmospheric composition, then it should also have other isotopes of argon, including ^{36}Ar. Because the proportion of ^{40}Ar to ^{36}Ar is constant in the atmosphere (295.5 to 1), a measurement of ^{36}Ar by the mass spectrometer can be used to determine the amount of atmospheric ^{40}Ar incorporated into the sample (McDougall and Harrison 1988).

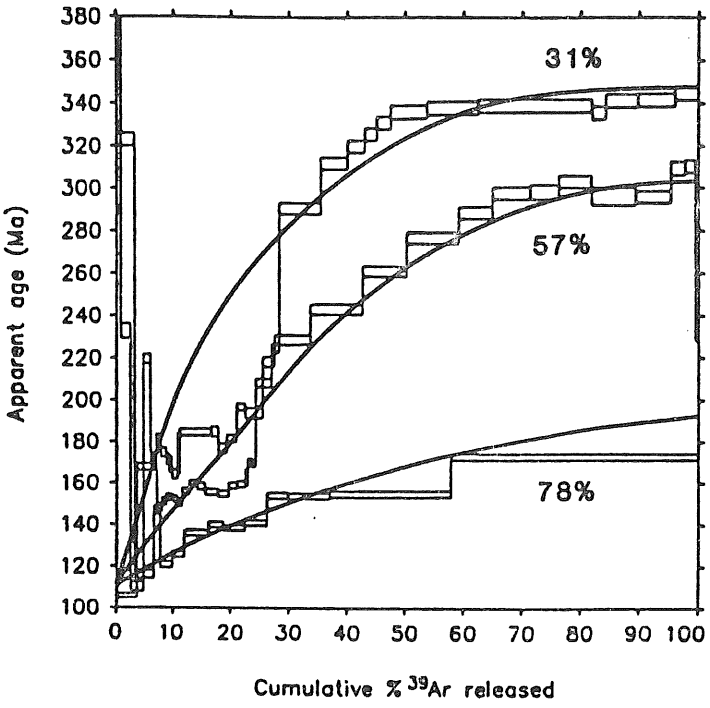

Fig. 2.4. Spectra disturbed by a short lived thermal event. The hornblende samples were taken from a gabbro. The plot displays three hornblende spectra which bear differing amounts of thermal resetting depending on their distance from a granite which intruded the gabbro. The top spectrum shows the least disturbance since it still bears a plateau. The lowermost spectrum shows the most resetting. The curved lines are theoretical lines made to match the data. From Hanes (1991).

The assumption that all non-radiogenic ^{40}Ar trapped within a mineral comes from the atmosphere is not valid, however. Often the trapped argon component has an $^{40}Ar/^{36}Ar$ ratio greater than 295.5, implying that the mineral incorporated ^{40}Ar from surrounding fluids (McDougall and Harrison 1988). Argon with an $^{40}Ar/^{36}Ar$ greater than 295.5 is called excess argon. Argon-enriched fluid escaping from deeper formations is a possible source of excess argon. Application of the ^{36}Ar atmospheric correction is obviously not appropriate for excess argon.

Why should a mineral take up excess ^{40}Ar? The previous discussions on slow cooling and short thermal events assumed that the geological environment of the mineral had a low ^{40}Ar concentration, promoting the diffusion of ^{40}Ar out of the crystal. If there were a high concentration of ^{40}Ar in the environment of the mineral, ^{40}Ar might diffuse into the crystal, providing the temperature was above the closure temperature (McDougall and Harrison 1988).

The presence of excess argon often is indicated by "saddle-shaped" spectra. Figure 2.5 displays a saddle-shaped spectrum, which records anomalously high ages in the first and last gas released. The lowest point in the middle represents the maximum closure age of the sample (McDougall and Harrison 1988; Harrison 1990). The incorporation of ^{40}Ar into the margins of the crystal easily explains why excess

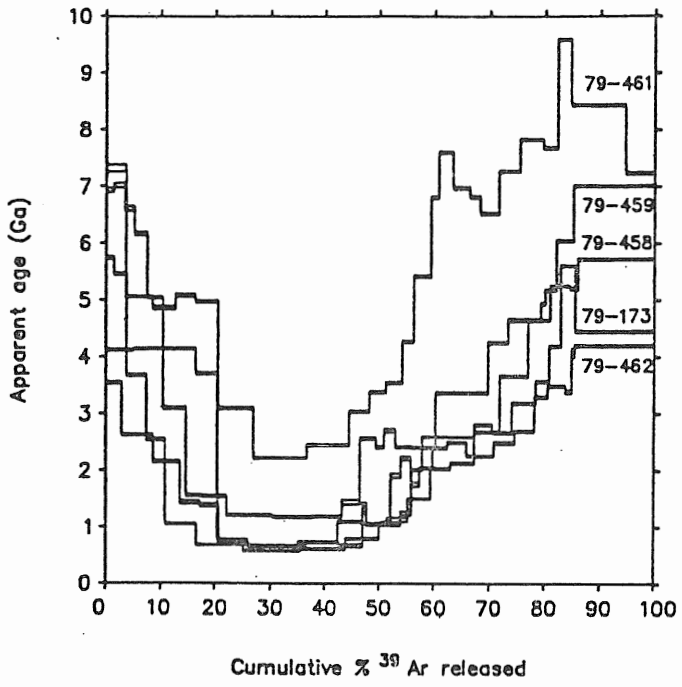

Fig. 2.5 Examples of excess argon from plagioclases. See text for description. From McDougall and Harrison (1988).

argon should appear in the first gas released because marginal sites discharge gas at relatively low temperatures during step heating.

The standard interpretation that higher temperature steps sample deeper portions of the crystal is inconsistent with the last few steps of gas containing excess argon. Harrison (1990) questions the notion that all spectra represent simple volume diffusion, especially for hydrous minerals such as hornblende. One obvious difference between the geological environment and the furnace environment is the time scale. Another important difference is that the samples in the furnace are heated in high vacuum, anhydrous conditions, while the geological environment is not subject to vacuum conditions and is most often hydrous. Because of these differences, Harrison claims that it is not reasonable to assume that a lattice site which easily accepts excess argon in the geological environment will just as easily release it in the heating furnace. This claim could help to explain why minerals containing excess argon have saddle-shaped spectra with a high age for the last gas released. Since spectra patterns may not be the result of volume diffusion only, the last gas released in the furnace is not necessarily a sample from the core, which seems to be an unlikely place for high concentrations of excess argon.

2.5 Inverse Isochrons

The inverse isochron diagram uses ratios of $^{39}Ar/^{40}Ar$ and $^{36}Ar/^{40}Ar$ displayed on the x-axis and y-axis respectively. The x-axis indirectly represents the age of the sample, with age increasing as the $^{39}Ar/^{40}Ar$ ratio decreases. The y-axis represents the composition of trapped argon component.

If all argon in a mineral is derived only from radioactive decay of ^{40}K, then there should be no ^{36}Ar in the mineral. The data from a step-heating analysis of this mineral would plot only on the x-axis of an inverse isochron diagram. Since the atmosphere and other sources of argon usually contain ^{36}Ar, and since many minerals incorporate external argon during formation or some other event, isotope data from most minerals will have a y-axis component.

If an assumption is made that the component of trapped argon has an atmospheric composition of $^{40}Ar/^{36}Ar = 295.5$ (or $^{36}Ar/^{40}Ar = 0.003384$) then a line can be drawn from this point on the y-axis to the sample point and then extrapolated through the x-axis (Fig. 2.6a). The $^{39}Ar/^{40}Ar$ value at the intersection of the x-axis and the line represents the parent-daughter isotope composition resulting from ^{40}K decay and can be converted to an age. This graphical function thus corrects for atmospheric argon contamination.

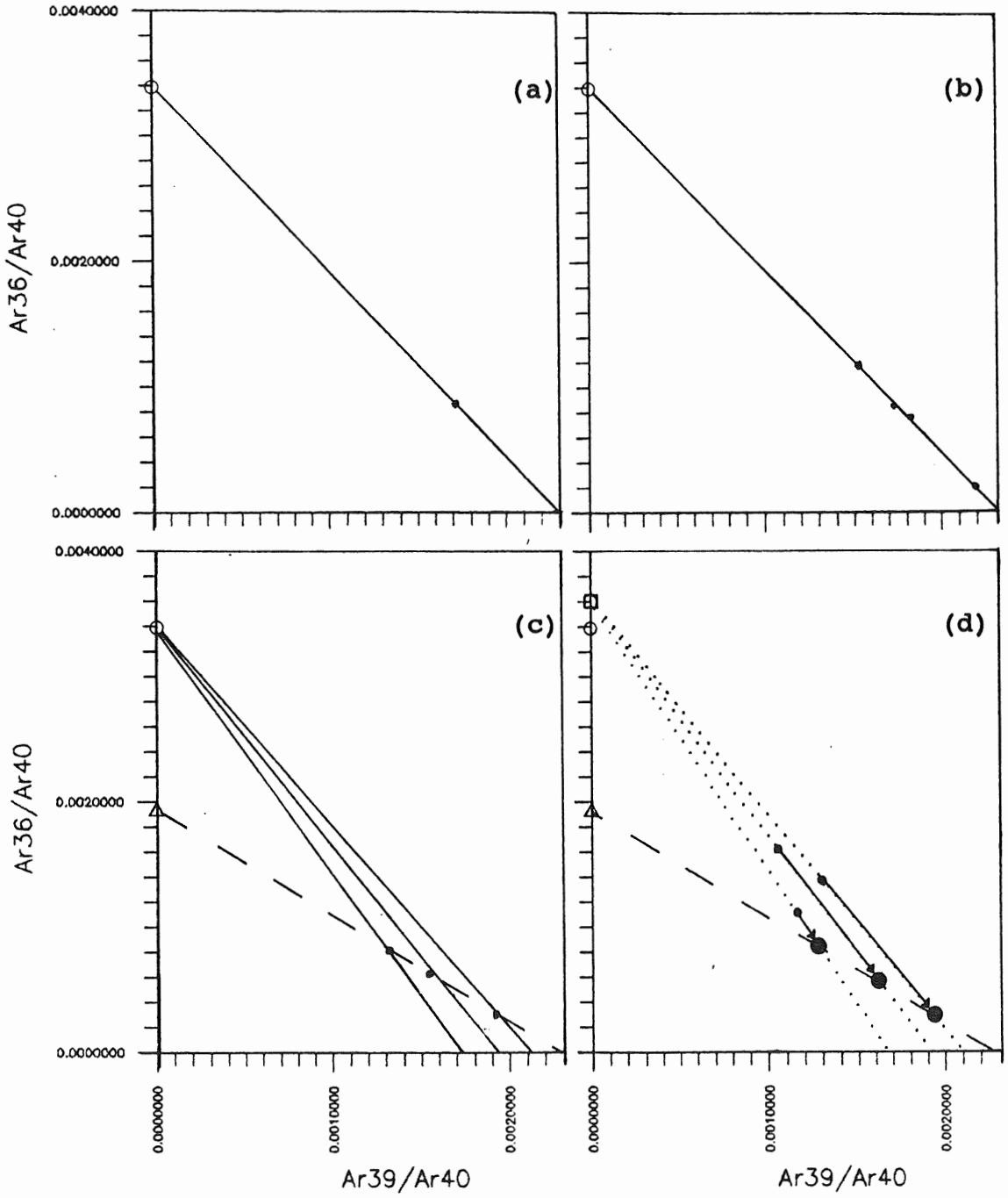

Fig. 2.6. Inverse isochron diagrams with hypothetical raw data (small solid circles). The data sets illustrate $^{36}Ar/^{40}Ar$ and $^{39}Ar/^{40}Ar$ isotope values which are: (a) uniform and have an assumed atmospheric trapped argon intercept (open circle), (b) collinear with atmospheric trapped argon intercept, (c) collinear with non-atmospheric trapped argon intercept (open triangle), and (d) non-collinear until blank corrected (large solid circles). See text for explanation.

In practice, the computer performs the same function when it calculates the age for each heating step.

If analysis of all heating steps for a sample have the same isotopic values, they will all define a point. The line connecting the y-intercept and the sample point can be extrapolated through the x-intercept, which yields a single age (Fig.2.6a). If different locations within the crystal contain varying proportions of trapped component to radiogenic component, but that trapped component has the same atmospheric composition no matter what its size, then the sample points should define a single line which passes through the atmospheric composition value on the y-axis (Fig. 2.6b) The extrapolated x-intercept yields a single age. An age spectrum constructed from the same sample data would be flat, because, as mentioned above, the computer linked to the mass-spectrometer performs this extrapolation function.

The two previous examples illustrate ideal situations, but usually the isotope data plotted on inverse isochron diagrams are complicated by trapped argon compositions differing from atmospheric values, and by contamination from the furnace system (blank). Often a mineral has a trapped argon component which is different from the atmospheric value (for example, excess argon, as discussed in Section 2.4.4, would plot lower on the y-axis). Figure 2.6c shows a set of data which define a line that intercepts the y-axis

at a $^{36}Ar/^{40}Ar$ value much lower than the atmospheric value (dashed line). The computer linked to the mass-spectrometer does not find a best fit line through the data, however, but corrects each step heating datum for atmospheric contamination. The effect of this computer operation is shown by the inverse isochron diagram in Figure 2.6c where a line is drawn between the atmospheric composition value on the y-axis and each heating step point, creating an array of lines with different x-intercepts (solid lines). The resulting age spectrum will appear disturbed, and unless an inverse isochron diagram is constructed, the sample results may be misinterpreted.

Another factor contributing to non-collinear inverse isochron plots is background contamination in the extraction furnace, called the blank. The walls of the furnace and connecting pipes degas during sample heating and may add a small argon component to the sample gas. The amount of blank is different for each temperature step, so the amount of contamination for each heating step of a sample varies. The data of a sample highly affected by blank contamination will appear non-collinear, as in Figure 2.6d (small solid circles).

In order to determine the blank, the extraction furnace is run empty, but on a standard heating schedule as if it contained a sample. This allows the argon degassed from the furnace and pipe walls to be collected and measured for each

temperature step. The analysis also yields the composition of the blank, which can be plotted on the inverse isotope diagram. Since the ^{39}Ar content of the blank is very low and is in practice assumed to be zero, the blank composition plots directly on the y-axis (Fig. 2.6d, open square). Tie-lines (dotted lines) connect the blank composition and the blank-contaminated sample data (small solid circles).

A proportion of the raw blank ^{36}Ar amount to the total raw sample ^{36}Ar amount determines the proportion of blank contamination for each heating step. Each sample datum is then "slid" along its tie-line by the amount of blank contamination for that heating step towards the x-axis (Fig.2.6d, arrows). Thus, the blank can be corrected for each heating step. The corrected data points (large solid circles) may be collinear, facilitating the extrapolation (dashed lines) of a y- and x-intercept.

Clearly, an age spectrum taken at face value may lead to misinterpretations resulting from the assumed trapped argon composition and blank contamination. However, it is worthwhile to bear in mind that usually the data points from the main outgassing steps plot very close to the x-axis, so that a change in orientation of the extrapolated lines will cause only a small change in value of the x-intercept (i.e. a change in the assumed trapped argon composition will produce a much smaller change in age). It is also quite possible that data from a step heating analysis of a mineral

sample will produce a scattered isochron plot even after blank correction. This means that the composition of the trapped argon is different depending on the location within the crystal, which may make accurate age determination impossible.

CHAPTER 3: SAMPLE METHODOLOGY

3.1 Sample Location

The eight sample locations on the 50 km long transect yielded 12 rock samples. The average distance between the locations perpendicular to strike was roughly 3 km. Note that Locations 6 and 8 have a wide distance between individual rock samples (Fig. 3.1).

3.2 Sample Description

Tables 3.1 and 3.2 record the location, sample numbers, and descriptions of the hornblendes and muscovites. Samples obtained from dykes and mafic gneisses yielded most of the hornblende. Hornblende was also obtained from gneiss of granitic and intermediate composition. Pegmatite dykes outcrop at all three sample locations in the CGB and contain abundant muscovite. The rarity of pegmatites hampered muscovite sampling in the GFTZ; micaceous bands within paragneiss at the westernmost sample location contain the only muscovite found in this part of the GFTZ.

The dykes and gneisses which provided the hornblende samples are LS tectonites. The average grain size of the hornblende ranges between 0.2 mm and 2 mm. All but two

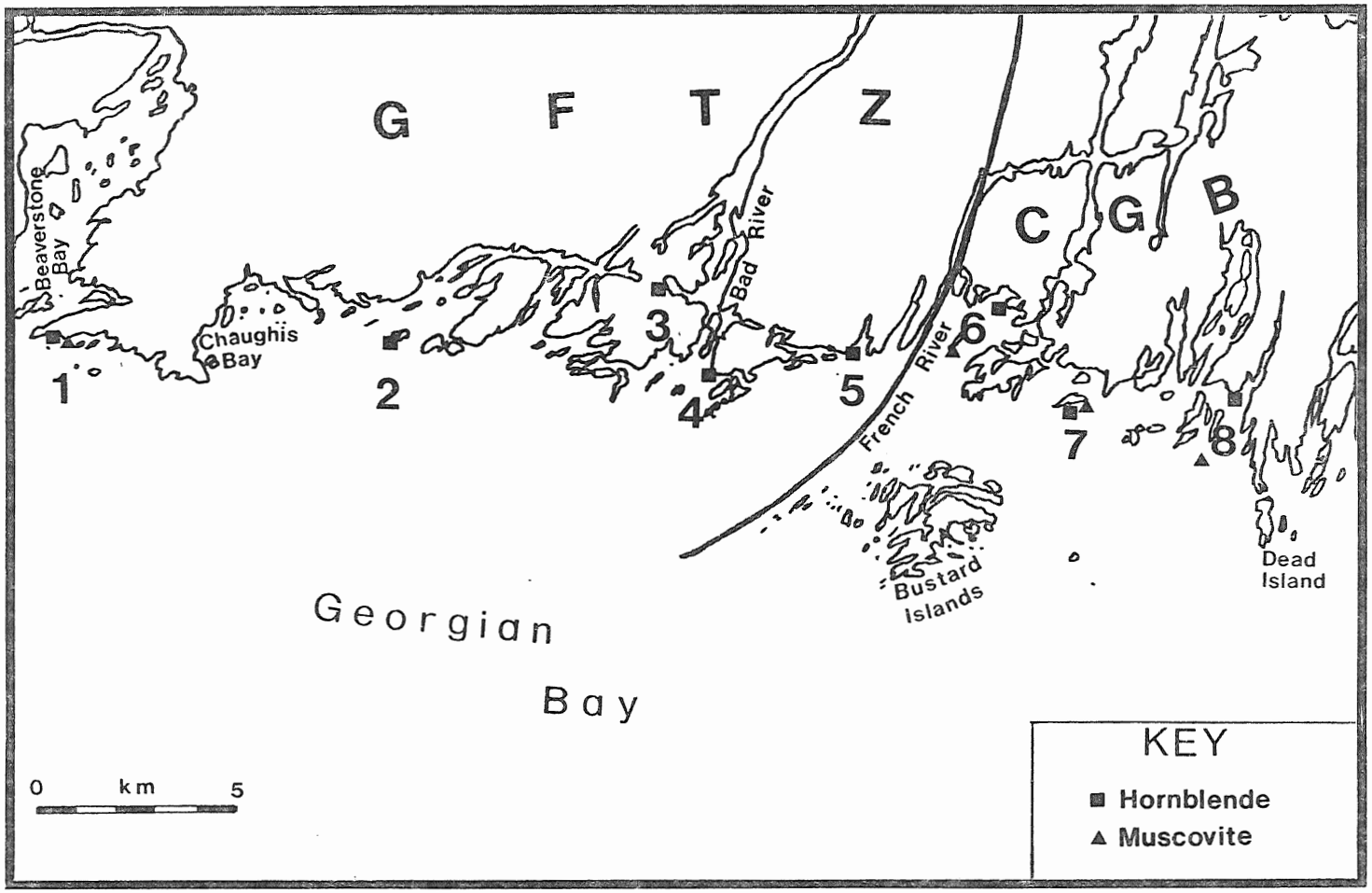

Figure 3.1. Sample locations of the transect.

SubProv-	(Location) sample #	rock description	mineralogy	comments
CGB	(8) ND-107A	Mafic gneiss	Pl,Qtz,Hbl, Bt,Aln	-anhedral Hbl -some Bt-Hbl intergrowth -Qtz,Bt,Aln inclusions in Hbl
	(7) ND-49C	Mafic dyke, foliated	Hbl,Bt,Qtz, Pl,Grn,Mag, Zrn	-subhedral Hbl -some Bt-Hbl intergrowth -Bt,Qtz,Mag inclusions in Hbl
	(6) ND-38A	Mafic gneiss	Hbl,Pl,Qtz, Kfs,Grn,Cal, Chl,Mag,Ttn, Zrn	-subhedral Hbl -no biotite -small clear inclusions in Hbl -Hbl altered to Chl
GFTZ	(5) ND-33	Hb-Bt-Qtz monzonite orthogneiss	Qtz,Pl,Ksp, Hbl,Bt,Mag, Zrn	-anhedral Hbl -Bt,Hbl in thin bands -Bt,Pl,Qtz inclusions in Hbl
	(4) ND-103	Hb-Bt-Qtz monzonite orthogneiss	Qtz,Pl,Ksp, Hbl,Bt,Mag, Zrn	-anhedral Hbl -Bt,Hbl in thin bands -Bt,Pl,Qtz inclusions in Hbl
	(3) ND-102C	Mafic dyke, foliated	Hbl,Pl,Qtz, Kfs,Mag,Zrn	-anhedral Hbl -no Bt -Qtz,Pl,Zrn inclusions in Hbl
	(2) ND-94B	Mafic dyke, foliated	Pl,Qtz,Hbl, Bt,Grn	-anhedral Hbl -some Hbl-Bt intergrowth -Bt,Qtz inclusions in Hbl
	(1) ND-91B	Mafic dyke, foliated	Hbl,Bt,Pl, Qtz,Chl,Ttn	-anhedral Hbl -Bt-Hbl intergrowth -Bt,Qtz,Ttn inclusions in Hbl

Table 3.1 Hornblende sample and parent rock descriptions. The following is a list of abbreviations used in the table: Aln = allanite, Bt = biotite, Cal = calcite, Chl = chlorite, Grn = garnet, Hbl = hornblende, Kfs = potassium feldspar, Mag = magnetite, Pl = plagioclase, Qtz = quartz, Ttn = titanite, and Zrn = zircon.

subprov	(Location) sample #	rock description	mineralogy	comments
C	(4) ND-107B	post tectonic pegmatite	Pl,Qtz,Ms, Cal,Ttn	-altered -Ms cloudy
G	(3) ND-49F	pegmatite	Qtz,Pl,Mc, Ms	-altered -Ms cloudy
B	(2) ND-38B	post tectonic pegmatite	Qtz,Or,Ms	-altered -Ms cloudy
GFTZ	(1) ND-91C	felsic gneiss	Pl,Mc,Qtz, Bt,Grn, trace Ms	-Ms scarce, only in thin layers

Table 3.2 Muscovite sample and parent rock descriptions. Abbreviations include: Bt = biotite, Cal = calcite, Grn = garnet, Mc = microcline, Ms = muscovite, Or = orthoclase, Pl = plagioclase, Qtz = quartz, Ttn = titanite.

samples contain biotite, which is commonly intergrown with or forms inclusions within hornblende.

Pegmatite dyke samples are coarse-grained and contain books of mica which have a grain size of 0.5 - 1.5 cm. The muscovite in the gneiss at Location 1 was fine grained (0.1 - 0.2 cm) and only occurred in a few thin (~1 cm) mica-rich bands.

3.3 Sample Preparation

3.3.1 Disaggregation

Ideally, disaggregation of the rock samples will liberate individual crystals so that subsequent separation procedures can effectively isolate crystals of one mineral type. The sample should not be broken down further than the grain size because this would upset any concentration gradients of ^{40}Ar or ^{40}K in the minerals (McDougall and Harrison 1988).

3.3.2 Hornblende separation

The biotite in some samples is tightly intergrown with hornblende. Because biotite is more K-rich than hornblende, it is especially important to separate these two minerals.

The eight rock samples (~10 to 20 cm) containing hornblende were broken down to 5 mm particles using a jaw-crusher. A tungsten-carbide rotary pulverizer reduced the

grain size of the sample. Washing the pulverized sample with water winnowed away very fine particulate matter, leaving the desired 0.1 to 0.5 mm sample grains.

The mafic components of samples ND-103 and ND-33 were concentrated using heavy liquid separation (sodium polytungstate) before the magnetic separation step. A Frantz magnetic separator divided the crushed samples into felsic and mafic fractions and also removed very magnetic particles such as small steel fragments (from the crushing devices) and magnetite.

Each hornblende grain was carefully hand-picked from the magnetic separate under a binocular microscope to ensure sample purity. Sample amounts ranged from 10 to 20 mg.

3.3.3 Muscovite separation

The mica books in the pegmatite samples were large, so that crushing and magnetic separation were not necessary. Large grains of muscovite (up to 5 mm width) were easily obtainable by plucking them out of the rock. Large muscovite books were split into thin layers for close examination. Many of the muscovite flakes were cloudy with small inclusions; only the clearest crystals were selected.

The small amount of muscovite contained in the felsic gneiss (ND-91C) was fine-grained and difficult to extract. Less muscovite was obtained for this sample (~1 mg).

3.3.4 Irradiation

All samples were wrapped in very pure aluminum foil and packed in a canister. After being bombarded by fast neutrons for 10 hours in the reactor at McMaster University, the canister was shipped back to Dalhousie University where it was allowed to cool.

3.4 Procedure in the Argon Lab

The argon analytical system consists of three basic units: the furnace, the mass spectrometer, and the computer. The furnace is constructed on the double vacuum principle; one vacuum compartment houses and protects the tantalum resistance coil, and the other vacuum compartment includes the extraction line in which the samples are heated and degassed. The extraction line includes: the heating compartment, which is surrounded by the resistance coil; the titanium "getter", which purifies the gas from the sample; the ion pump, which maintains a vacuum in the system; and several valves, which control the movement of gas to the ion pump and the inlet of gas into the mass spectrometer.

A sample placed within the furnace is normally heated for 20 minutes at a particular temperature, during which time argon and other gases are released. Before the gas is admitted into the mass spectrometer, the titanium getter is

allowed to work for ten minutes to purify the argon gas. Once the gas has moved into the mass spectrometer, the furnace line ion pump is activated to clean the system of the sample gas, preparing the furnace line for a new sample.

The argon gas which is now in the mass spectrometer is measured and the argon isotopic ratios $^{40}Ar/^{39}Ar$, $^{36}Ar/^{39}Ar$, and $^{37}Ar/^{39}Ar$ are calculated. The computer uses the $^{40}Ar/^{39}Ar$ ratio to calculate the age of the sample after corrections are made for atmospheric argon contamination and interfering isotopes using $^{36}Ar/^{39}Ar$ and $^{37}Ar/^{39}Ar$ respectively. The data are stored in the computer.

After the ion pump on the furnace line has cleaned the old sample gas out of the system, the temperature is raised and the mineral sample heated again. A sample normally undergoes several cycles of incremental temperature increase during a standard analysis. This process is known as step heating. Eventually a temperature is reached where the mineral is completely outgassed and the run is stopped.

3.5 Microprobe Preparation

Because biotite was present in most of the rock samples which provided the hornblende, polished thin sections of the hornblende-containing samples were prepared for microprobe analysis. On each thin-section, three hornblende minerals

were analyzed. The Ca/K ratio of the hornblende is of particular interest because it can help to determine the extent of biotite contamination when compared to the isotope data from the mass-spectrometer.

CHAPTER 4: RESULTS

4.1 Age Spectra Results

4.1.1 Hornblende

Figures 4.1 and 4.2 locate the sample sites of the hornblende spectrum diagrams. Each spectrum diagram contains the age spectrum (open bars) and the $^{37}Ar/^{39}Ar$ ratios (solid bars) determined for each sample by the argon analytical system. Each range marker (labelled "microprobe") displays the $^{37}Ar/^{39}Ar$ ratio converted from the microprobe Ca/K ratio for ease of comparison. The summary sheets of the argon analytical system results and the microprobe results appear in Appendix 1.1 and Appendix 2 respectively.

The ages of the five easternmost hornblende samples range from 995 Ma to 1016 Ma (Figs. 4.1 and 4.2). An older age grouping at the western end of the transect comprises sample ND-94B with an age of 1120 Ma flanked by samples ND-102C and ND-91B with somewhat younger ages. The first step of gas release for each hornblende spectrum except ND-94B and ND-38A records an anomalously high age, or "spike".

Two hornblende spectra, those of samples ND-91B and ND-94B, fail to meet the criteria for a plateau (Fleck et al. 1977). The modified total gas age (TGA) of sample ND-91B (Fig. 4.1) is a weighted average of all heating steps except for the first and last few steps, which are anomalously

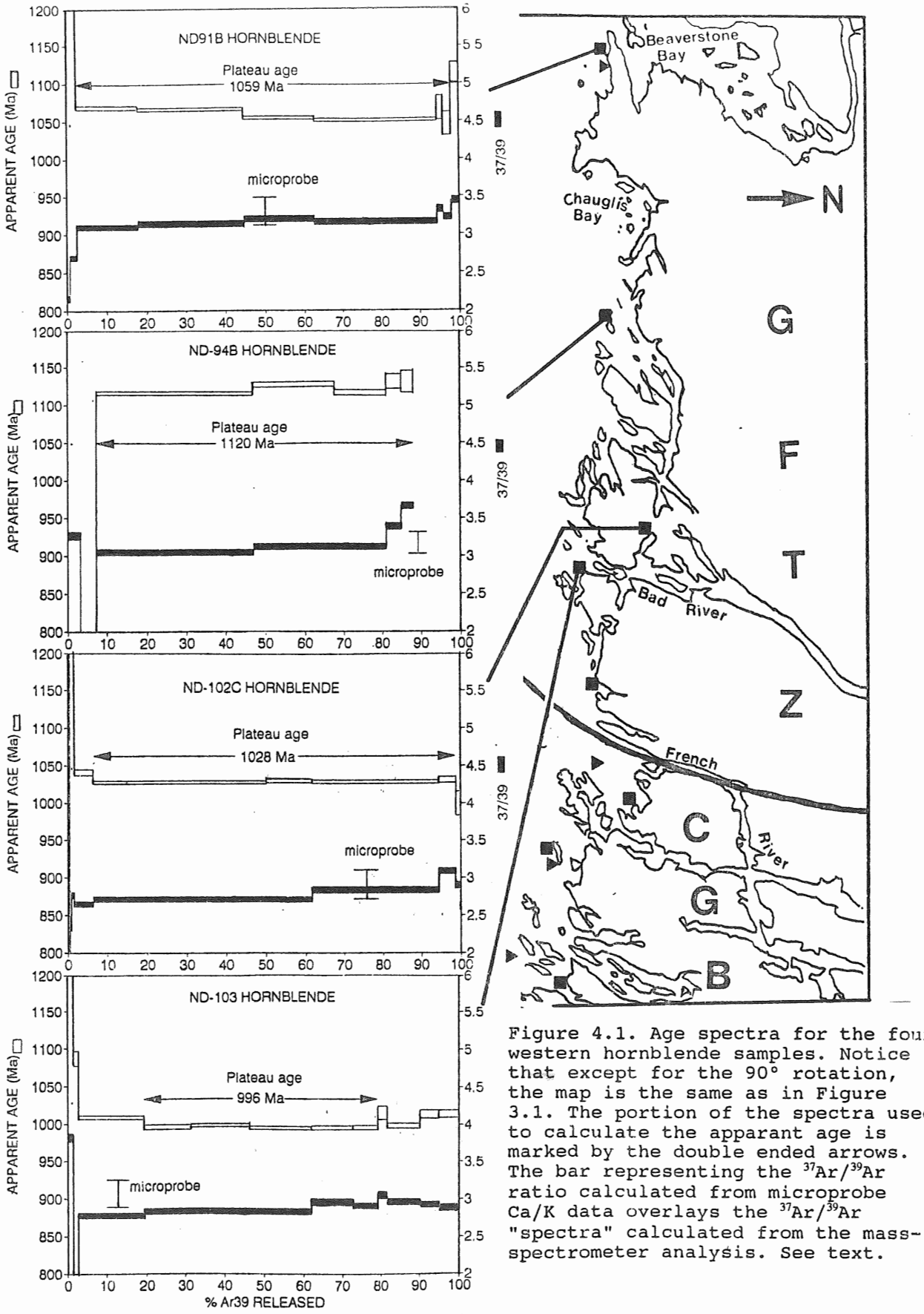

Figure 4.1. Age spectra for the four western hornblende samples. Notice that except for the 90° rotation, the map is the same as in Figure 3.1. The portion of the spectra used to calculate the apparant age is marked by the double ended arrows. The bar representing the $^{37}Ar/^{39}Ar$ ratio calculated from microprobe Ca/K data overlays the $^{37}Ar/^{39}Ar$ "spectra" calculated from the mass-spectrometer analysis. See text.

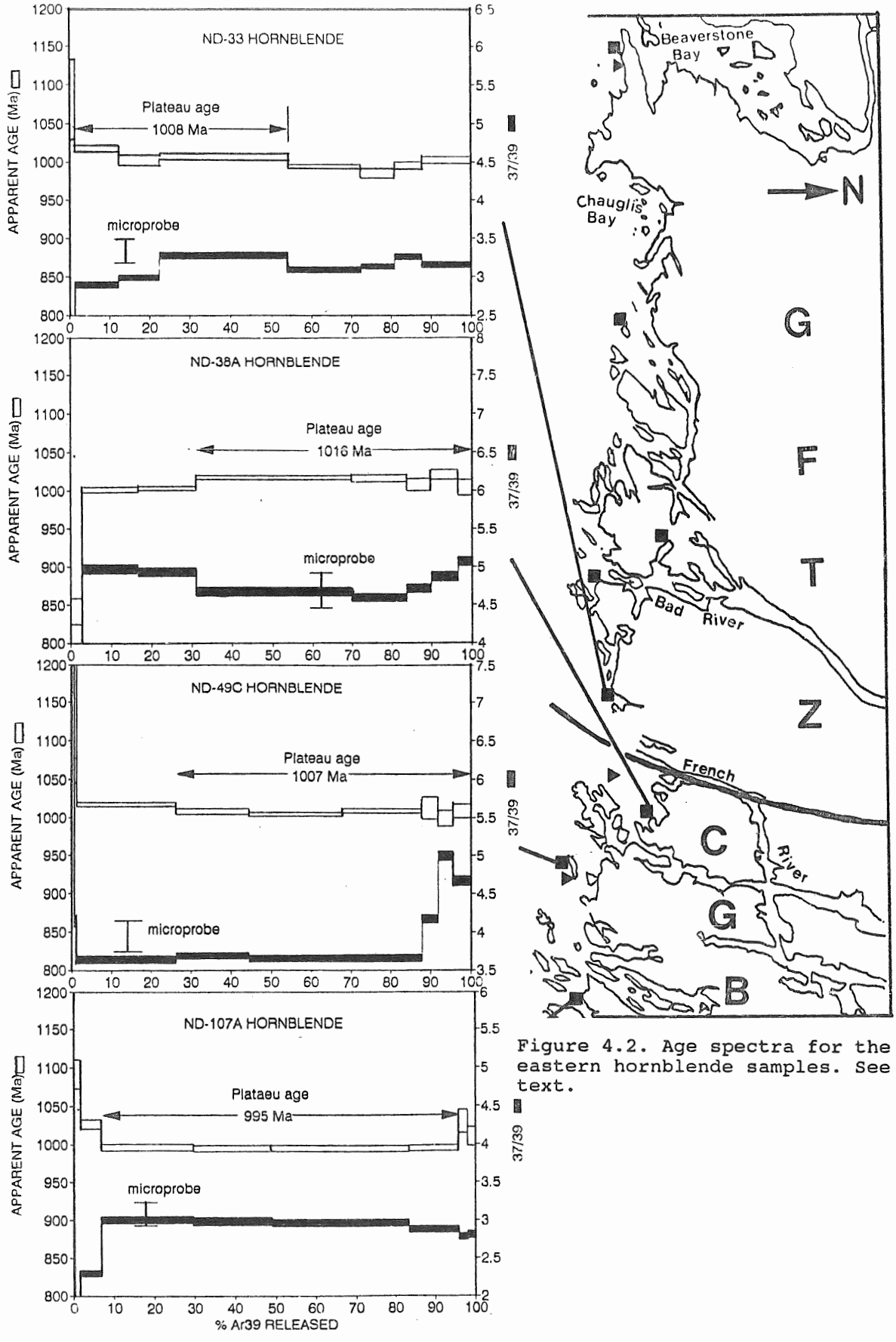

Figure 4.2. Age spectra for the four eastern hornblende samples. See text.

high. The central portion of the spectrum used to calculate the modified TGA represents 96% of the total gas released.

The modified TGA of sample ND-94B does not include the first two steps, representing about 7% of the total gas released, because they have anomalously low ages (Fig. 4.1). The spectrum for ND-94B is not complete because the final steps of gas suffered contamination. Figure 4.4 summarizes the hornblende spectra results.

4.1.2 Muscovites

Figure 4.3 locates each muscovite age spectrum on the adjacent map (Appendix 1.2 contains the muscovite data summary from the argon analytical system). The three muscovites from the eastern end of the transect have very similar ages, ranging from 930 Ma to 933 Ma. Sample ND-91C, at the western end of the transect, has a much older age of 1112 Ma.

The muscovites generally yielded spectra with more consistent ages than the hornblendes (Fig. 4.3). Samples ND-38B and ND-49F yield plateaux which account for over 90% of the gas released. The plateau for ND-91C represents 75.8% of the gas released. Also, ND-91C contains fewer but larger gas release steps. The small mass of sample ND-91C (~1 mg) required larger temperature increases between steps in order to ensure that each gas portion was large enough for accurate measurement.

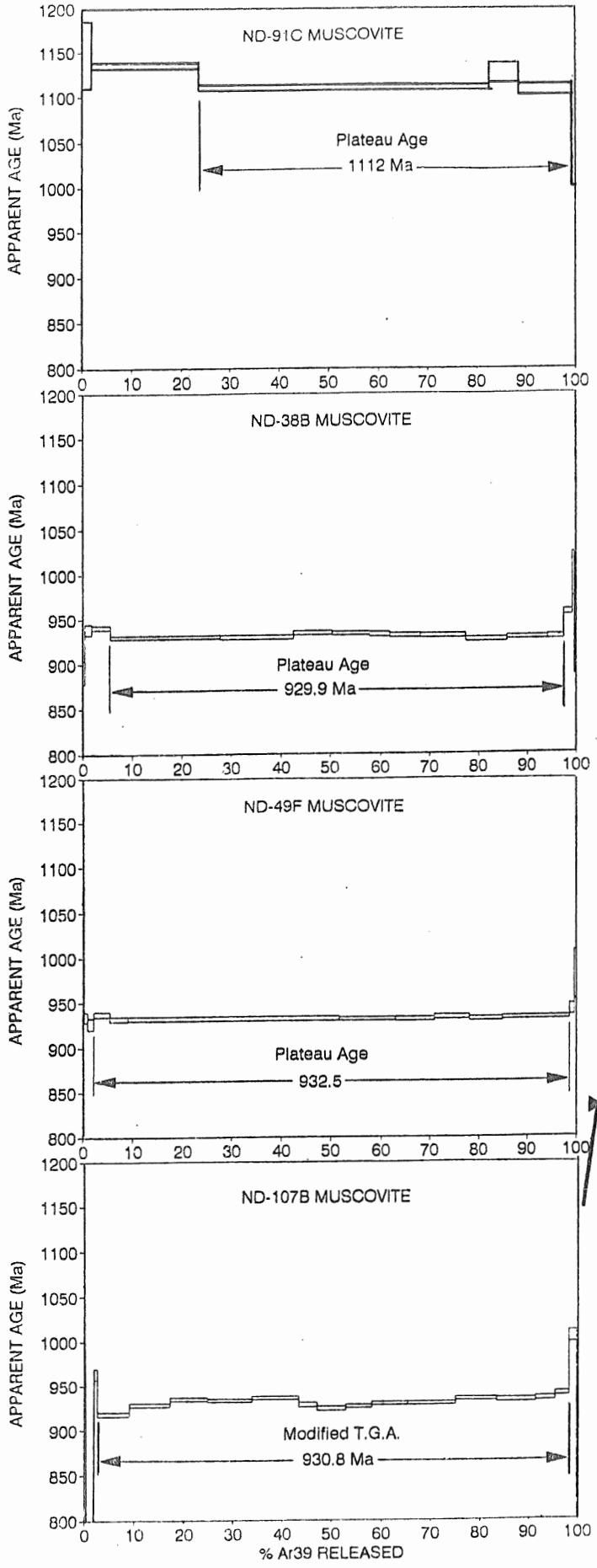

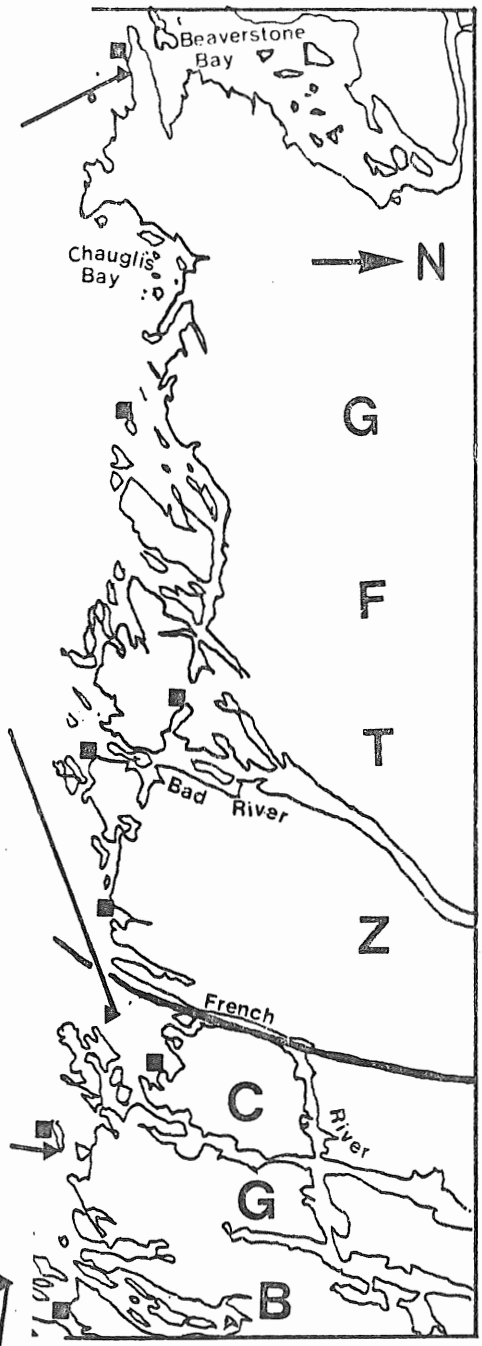

Figure 4.3. Muscovite age spectra.

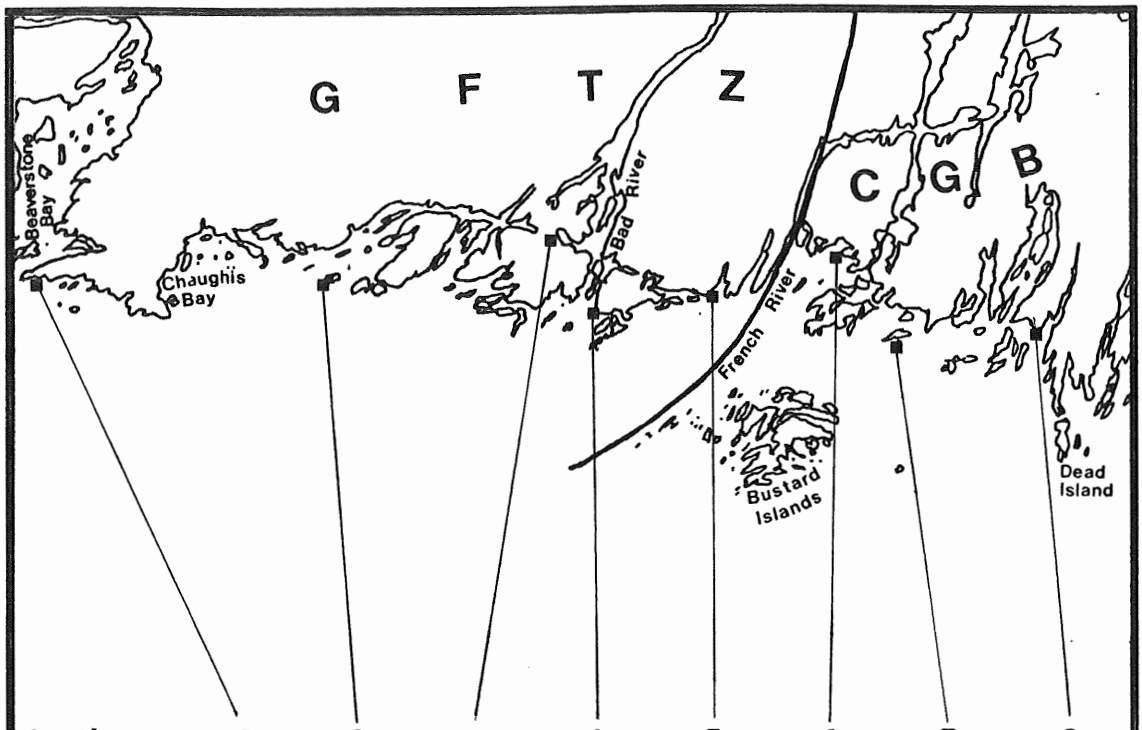

Location / sample ND-	91B	94B	102C	103	33	38A	49C	107A
age (Ma)	1059	1120	1028	996	1008	1016	1007	995
error (Ma)	± 13	± 14	± 13	± 12	± 12	± 13	± 12	± 12
age type	mod. TGA	mod. TGA	plat.	plat.	plat.	plat.	plat.	plat.
percent of gas	95.2	77.4	92.1	59.7	52.6	69.7	73.6	88.9
first gas	high	low	high	high	high	low	high	high
last gas	high?	–	–	high?	high?	–	high?	high?
saddle	yes	no	no	yes	yes	no	yes	yes

Figure 4.4. Summary of spectra results from hornblendes. The solid squares on the map show the locations of the hornblende samples. The row labelled, "percent of gas" refers to the percentage of gas contained in the steps used to calculate the plateau age or TGA. The abbreviation "mod. TGA" stands for modified total gas age and "plat." stands for plateau age.

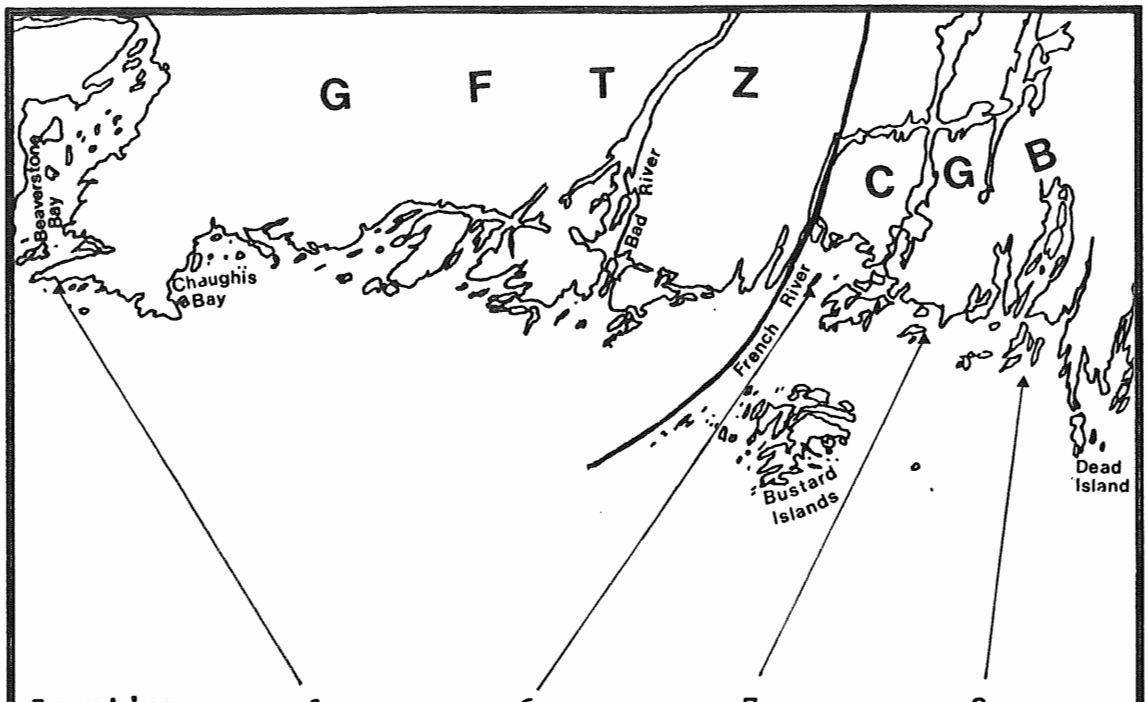

Location / sample ND-	91C	38B	49F	107B
age (Ma)	1112	930	933	931
error	±14	±12	±12	±12
age type	plateau	plateau	plateau	modified TGA
percent gas	75.8	91.6	96.4	95.1

Figure 4.5. Summary of spectra results from muscovites. The solid triangles show the location of the muscovite samples. The row labelled, "percent gas" records the percent of gas contained in the steps which were used to calculate the age.

The spectrum for sample ND-107 contains no plateau; however, the variation among all but the first two and last two steps is not great, so a weighted average of the central portion of the spectrum ages is appropriate. Because the weighted average excludes the first two and last two steps, it is called a modified TGA (Fig. 4.3).

The muscovite spectra in general are undisturbed, thus the plateau age or modified TGA will be adopted as their time of cooling. Figure 4.5 summarizes the spectra results of the muscovites.

4.2 Discussion of Hornblende Spectra

4.2.1 High ages of first and last gas released

All of the hornblende spectra, except those for samples ND-94B and ND-38A, have anomalously high ages, or "spikes", in the first few percent of gas released (Figs. 4.1 and 4.2). Both ^{39}Ar recoil (Section 2.3.3) and excess argon (Section 2.4.4) can produce a spike in the first gas. Determining which effect produced the spike is not important because the calculation of plateau or modified TGA ages does not use the anomalously high ages represented by the spike. Likely, however, both ^{39}Ar recoil and excess argon contributed to the anomalously high ages in the first gas released. Figure 4.4 summarizes the spectra interpretations.

4.2.2. Saddle-shaped spectra

If the high-age spikes are ignored, most of the hornblende spectra are relatively flat, but ND-91B, ND-103, ND-33, ND-49C, and ND-107A have a slight saddle (Figs. 4.1 and 4.2; Fig. 4.4 for summary). In theory, the low point of the "saddle" represents the maximum age of the sample because the older apparent ages suffer from excess argon (Section 2.3.2).

The plateaux for ND-103, ND-49C, and ND-107A include the step with the lowest age. Because older steps on either side of the lowest-aged step were incorporated into the weighted average, the plateau age is older than the maximum age. The saddle effect is slight (the differences among all the steps within the plateau are less than 5 million years), so the weighted average is not significantly higher than the maximum age. The flatness of the saddles also indicates that the maximum age should nearly equal the true cooling age.

The modified TGA of 1059 Ma calculated for sample ND-91B comprises greater than 95% of the gas released. The steps with the lowest age in the saddle-shaped spectrum have an age of ~1053 Ma and represent the maximum age. The plateau for sample ND-33 (1008 Ma) does not include the low point of the saddle, which represents a maximum age of 984 Ma.

In most cases the saddle-shape is not very pronounced. The high ages for the first gas released are not necessarily

caused by excess argon (part of the high age could be the result of ^{39}Ar recoil), and no samples portray a convincing rise in age for the last gas released. Because the interpretation of saddle-shaped spectra is debatable, this thesis adopts plateau ages or modified TGA. Inverse isochrons (Section 4.3.2) may help determine the nature and extent of excess argon contamination.

4.2.3 Low ages for the first gas released

Two samples have low ages for the first gas released. The spectrum for sample ND-38A contains one step with an age of 850 Ma which represents ~3% of the gas released. The first two steps of sample ND-94B total ~7% of the ^{39}Ar released and have ages of 530 Ma and 618 Ma. Two possible causes for this type of profile are thermal resetting (Section 2.4.3) and slow cooling (Section 2.4.2). The ~575 Ma Grenville dykes, which occur north of the transect, (Fahrig and West 1986) are a possible candidate for thermal resetting, but there is no apparent reason why only ND-94B and ND-38A were affected by the thermal event. The sudden shift in ages from the first two steps of the spectrum to the main phase of gas release does not resemble the more gradual transition displayed by the spectra of slowly cooled or thermally reset samples.

4.3 Validity of Spectra

4.3.1 Comparison of ages

The simplest test of $^{40}Ar/^{39}Ar$ age validity is a comparison of results from different minerals. Since hornblende has a higher closure temperature than muscovite, muscovite should never have an older age than hornblende from the same location since hornblende would reach closure temperature first during cooling.

Sample Locations 6, 7, and 8 in the Britt Domain of the CGB each have a muscovite - hornblende pair. In these three cases the results are geologically reasonable; the average age of the hornblendes is ~1005 Ma and the average age of the muscovites is ~930 Ma. The ~75 million years difference between the ages of the two minerals is comparable to results by Culshaw et al. (1991) to the east in the Britt Domain.

Only Location 1 (ND-91B) in the GFTZ has a muscovite to compare with the hornblende results. The 1059 Ma age of the hornblende sample is significantly younger than the 1112 Ma age of the muscovite. This unreasonable situation casts doubt over both of these ages, even though both the hornblende and the muscovite spectra meet the plateau requirements of Fleck et al. (1977) and seem well behaved. Further tests of hornblende validity may reveal problems with hornblende ND-91C.

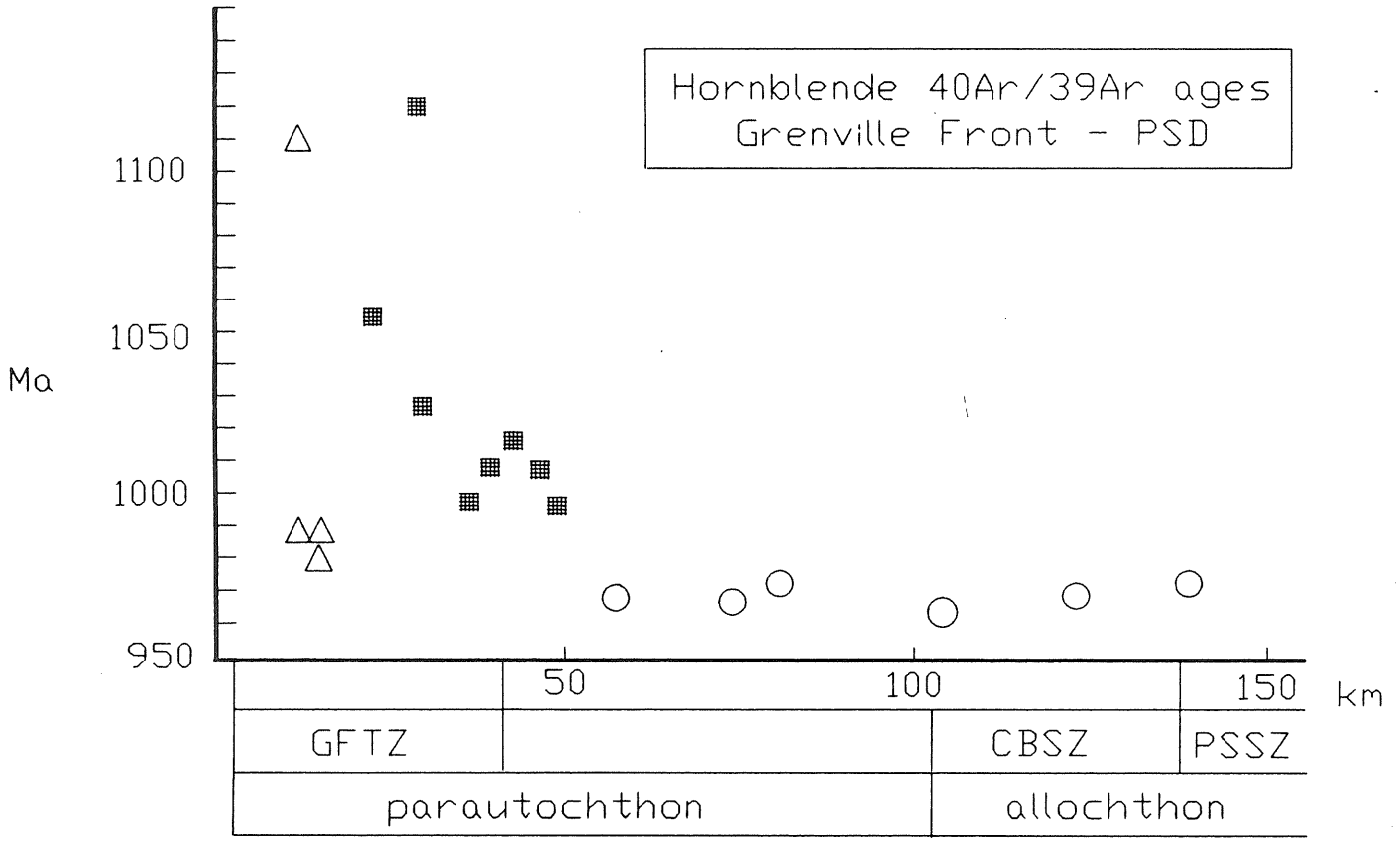

Figure 4.6. Age verses distance across northern Georgian Bay. The x-axis represents the distance in kilometres east from the Grenville Front. The hachured squares present the data of the present transect. The open triangles and circles represent the results of Culshaw et al. (1991) and Haggart (1991) respectively.

Within the group of hornblendes with high ages on the western edge of the transect, including samples ND-91B, ND-94B, and ND-102C, the ages vary considerably (Fig. 4.6). Also, the samples on the eastern edge of the present transect and the samples on the eastern edge of the transect studied by Haggart (1991) have very similar ages (Fig. 4.6). While the structural location of the high ages may involve a tectonic explanation, the situation may also indicate that the age interpretations of the spectra are not valid, perhaps as a result of the presence of excess argon.

4.3.2 Ca/K ratios and K-content of hornblende

Biotite contains 7-8% structural K by mass, compared to a maximum of 2% for hornblende (Appendix 2.2). Biotite also often contains excess argon, so relatively small inclusions of biotite in hornblende could increase the apparent age of the samples. $^{40}Ar^{*}/^{39}Ar$ studies to the east in the Britt Domain by Check (1989) show that biotites recorded higher apparent ages than hornblendes from the same location. Check (1989) believed that excess argon was the cause of the high biotite ages. Another study by Easton (1986) documents excess argon in biotites near the Grenville Front.

Hand-picking eliminates most of the biotite and hornblende-biotite intergrowths, but small inclusions of biotite in hornblendes may go undetected. Petrography (Table 3.1) reveals that the hornblendes are sometimes intergrown with biotite and also contain small amounts of biotite

inclusion. A comparison between Ca/K in the hornblendes and Ca/K in the gas extracted by the furnace may help to assess whether the biotite inclusions in the hornblendes pose a serious contamination problem.

For each sample, repeated microprobe analyses of clear, unaltered spots within hornblende yielded consistent results (Appendix 2.1, Appendix 2.2), so the Ca/K ratios derived from the microprobe data should reflect the composition of the hornblende. Using a constant specific to the reactor at McMaster University [$Ca/K = 1.9(^{37}Ar/^{39}Ar)$], the Ca/K ratio from the microprobe data was converted to a $^{37}Ar/^{39}Ar$ ratio and plotted on Figures 4.1 and 4.2 for easy comparison with the argon analytical system $^{37}Ar/^{39}Ar$ data. An estimate of the error of the Ca/K ratio is 5% (R.M. Mackay, pers. comm. 1992).

The $^{37}Ar/^{39}Ar$ ratios derived from the argon analytical system reflect the Ca/K composition of all the material heated in the furnace; any inclusions of biotite or other matter in the hornblende samples will degas and mix with the gas derived from hornblende. Biotites have higher K-contents than hornblendes, so the Ca/K ratio of a hornblende contaminated with inclusions of biotite will be lower than a pure hornblende.

The major gas release portions of the $^{37}Ar/^{39}Ar$ "spectra" determined from the argon analytical system fall within the error of the $^{37}Ar/^{39}Ar$ ranges calculated from the

microprobe Ca/K ratios. Note that for almost all samples, the $^{37}Ar/^{39}Ar$ ratios derived from argon isotopes occupies the lower portion of the microprobe error range. The consistency of the slightly lowered $^{37}Ar/^{39}Ar$, and thus Ca/K, ratios from argon isotopes among geologically widely separated samples indicates that a calibration factor (for the microprobe or for the reactor conversion process) may be responsible. The absence of any significant difference between the Ca/K ratios from the mass spectrometer and the microprobe suggests that biotite contamination is negligible.

The K_2O-content of hornblende can also be used to test for the likelihood of excess argon. The total amount of K, and thus the total amount of radiogenic ^{40}Ar, may vary among adjacent hornblendes samples without affecting the $^{40}Ar/^{40}Ar$ ratio determined in the argon analytical system. Excess argon, largely ^{40}Ar, will interfere with the $^{40}Ar/^{39}Ar$ ratio to different degrees depending on the total amount of radiogenic ^{40}Ar contained within the mineral. For geographically adjacent samples of uniform age with varying amounts of total K_2O to have suffered excess argon contamination is very unlikely, since that would require each mineral to incorporate a different amount of excess argon. Not only would each mineral need incorporate a different amount of excess argon, but the exact amount of excess argon necessary to produce a $^{40}Ar/^{39}Ar$ ratio similar to neighbouring samples.

The K_2O content determined for the hornblendes of the transect varies between 1.7% and 1.0% (Appendix 3.1). The CGB samples and the two easternmost GFTZ samples (ND-103 and ND-33) lie adjacent to one another and have the same apparent age within error (Fig. 4.4) but have varying K_2O content. Following the argument in the previous paragraph, excess argon contamination seems unlikely. The three westernmost hornblendes have widely varying ages, thus the test is not applicable to these samples.

4.3.3 Inverse isochrons

The inverse isochron graphs (Appendix 3, top graph on each page) display the blank-corrected $^{36}Ar/^{39}Ar$ values plotted against $^{39}Ar/^{40}Ar$ values. The data clusters, so the portion of each graph containing the data has been expanded to a larger scale (Appendix 3, bottom graph on each page). Four plots display a linear character. Linear regressions for ND-94B, ND-102C, ND-33, and ND-49C yield x-intercepts, from which ages have been calculated; and y-intercepts, from which the initial $^{40}Ar/^{36}Ar$ compositions have been calculated. (Table 4.3). Notice that the ages derived from the isochron plots are very similar to the ages from the spectrum plots. The $^{40}Ar/^{36}Ar$ ratios of the trapped argon (Table 4.3), determined from y-intercepts of the inverse isochrons, are greater than atmospheric argon ($^{40}Ar/^{36}Ar$ = 295.5), implying that the trapped argon component is enriched in ^{40}Ar.

sample	ND-94B	ND-102C	ND-33	ND49C
correlation coefficient	-0.86	-0.99	-0.66	-0.88
intercept age (Ma)	1114 Ma	1028 Ma	1006 Ma	1005 Ma
initial $^{40}Ar/^{36}Ar$	3391	367	1141	747
spectra ages	1120 Ma	1028 Ma	1008 Ma	1007 Ma

Table 4.1 Results from isochron plots.

While the total amount of ^{36}Ar contamination is low (indicated by clustering of the data near or on the $^{39}Ar/^{40}Ar$ axis), the amount of ^{40}Ar contamination may still be quite high since the composition of the trapped argon may have been nearly all ^{40}Ar (supported by the high $^{40}Ar/^{36}Ar$ ratios determined from the extrapolated y-intercepts, although the error in the extrapolation is very high at the y-intercept). Excess argon containing very low amounts of ^{36}Ar would cause the $^{39}Ar/^{40}Ar$ ratio to decrease (and the calculated age to increase), pulling the data towards the origin along the x-intercept, without creating a large y-axis component.

Section 2.5 discusses inverse isochron diagrams as a means of delineating excess argon gradients within hornblendes; gradients of argon composition may be created by preferential incorporation of excess argon in the crystal margins. Although for four samples the data allowed the plotting of regression lines, it should be noted that the data clustered near the x-axis. Only a large magnification in scale produced delineation of the data and the small differences in values may be more a result of noise in the analytical equipment than a result of any excess argon gradient in the crystal.

CHAPTER 5: GEOLOGICAL INTERPRETATIONS

5.1 Excess Argon

The five eastern hornblende samples of the present study, ND-103, ND-33, ND-38A, ND-49C, and ND-107A do not seem to exhibit signs of serious excess argon contamination for the following reasons:

1) Sample locations within the GFTZ (hornblende samples ND-38A, ND-49C, and ND-107A) have muscovites with a younger, consistent age of ~930 Ma,

2) The five eastern hornblendes have ages which range between 1016 ± 13 Ma and 995 ± 12 Ma, constituting a relatively consistent age group, and

3) The ages of five eastern hornblendes are slightly older than the ages of the ~970 Ma hornblendes to the east (Check 1989 and Culshaw et al. 1991) and similar to the 979-996 Ma hornblendes to the west of Beaverstone Bay (Haggart 1991).

The five eastern samples have older ages than the hornblendes sampled immediately to the east by Check (1989) and Culshaw et al. (1991). The slight discrepancy of ages may be a result of low levels of excess argon contamination in the five eastern samples of the present transect. Alternatively, a tectonic break could explain the difference since there is very little evidence indicating excess argon.

Samples ND-94B, ND-91B, and ND-102C have ages of 1059 Ma, 1120 Ma, and 1028 Ma respectively. Excess argon is likely the cause of the elevated apparent ages based on the following evidence:

1) Sample ND-91 contains muscovite considerably older than the hornblende, which is geologically unreasonable,

2) The ages of ND-91B, ND-94B, and ND-102C, three adjacent locations, vary considerably, and

3) The ages of hornblendes to the west and to the east of ND-91B, ND-94B, and ND-102C range between about 1015 Ma and 970 Ma and are more consistent between adjacent locations.

Studies along Georgian Bay by Check (1989) and Culshaw et al. (1991) confirm the proposal by Roddick et al. (1980) that muscovites are less susceptible to excess argon contamination than biotite. The present study strongly suggests, however, that excess argon contaminates muscovite ND-91C, as well as the three "older" hornblendes. If excess argon artificially inflates the age of the hornblendes at Locations 1, 2, and 3 then the true $^{40}Ar/^{39}Ar$ age is lower. The ~985 Ma age of cooling at the western end of the transect studied by Haggart is very similar to the ages at Locations 4 to 8 of the present transect. Perhaps a uniform hornblende cooling age of ~995 Ma stretches across the whole area and the elevated age group (Locations 1, 2, and 3) represents excess argon contamination only. Alternatively,

the three hornblendes could possess an age different from that of the hornblendes to the west and east and still contain excess argon.

The proposal of excess argon contamination in the western end of the transect is mainly supported by age evidence. Other indicators of excess argon, such as saddle-shaped spectra, Ca/K ratio comparisons, and inverse isochron plots, were of little use in revealing the extent of excess argon contamination.

The saddle-shaped spectra are not found exclusively among the three western hornblendes with older apparent ages. Hornblendes ND-103, Nd-33, Nd-49C and ND-107A in the CGB have a slight saddle-shape even though they are not otherwise suspect. Hornblendes ND-94B and ND-102C in the western GFTZ have no saddle-shape even though they are highly suspect. Thus, for this transect, saddle-shapes are not a good indicator for the presence of excess argon.

One reason why hornblendes with excess argon may not possess saddle-shaped spectra involves the distribution of excess argon in the mineral. A saddle-shaped spectrum, in theory, displays older apparent ages in the first steps of gas release because of higher amounts of excess argon concentration in surface lattice sites. It is possible, however, that excess argon be incorporated into a mineral uniformly in which case, no tell-tale saddle-shape would be produced. The absence of saddle-shapes, as well as the

clustering of data on inverse isochron plots, may indicate uniform distribution of excess argon in the western hornblendes.

The high $^{40}Ar/^{36}Ar$ trapped argon ratios, as determined by the y-intercepts on inverse isochron diagrams, belong to both the western grouping (containing excess argon) and the eastern grouping (not containing excess argon). Little faith can be placed on the calculated ratios largely because the regression lines are based on relatively clustered data. Thus, for the present study, inverse isochrons are of little value in determining the extent of excess argon contamination. The clustering may indicate, however, that excess argon is concentrated uniformly throughout the crystal.

The $^{37}Ar/^{39}Ar$ graphs indicate that biotite, which very often contains excess argon, does not contaminate the hornblendes. Excess argon can contaminate hornblende directly, however, so the absence of biotite does not preclude the presence of excess argon in hornblendes.

5.2 Cooling and Exhumation History

The use of thermochronological data to determine cooling and exhumation history depends on several assumptions; these are:

1) The data must represent a real geological event;

minerals which have suffered excess argon contamination are not good candidates,

2) The closure temperature used for the mineral must be accurate, and

3) All samples used for data within an area must have undergone the same geologic history throughout the duration of cooling.

Samples ND-91B, ND-94B, and ND-102C (Locations 1, 2, and 3) suffered excess argon, thus they were not used for cooling calculations. The five remaining hornblendes appear to contain much less excess argon, so their use is appropriate. The ages of the five eastern hornblendes are consistent, as are the ages of the three muscovites, so the area containing the samples likely acted as a whole.

A compilation by Hanes (1991) provides the closure temperatures used for cooling calculations (Table 2.1). The range of temperatures for each mineral is high, but without experimentation to determine the closure temperatures directly for the hornblendes used in the present study, some reasonable estimation must be adopted.

Each of the three sample locations within the Britt Domain (Locations 6, 7, and 8) has a hornblende-muscovite pair, which was used to calculate a portion of a cooling curve (Fig. 5.1). Additional mineral ages from nearby studies were required to fill out the data set.

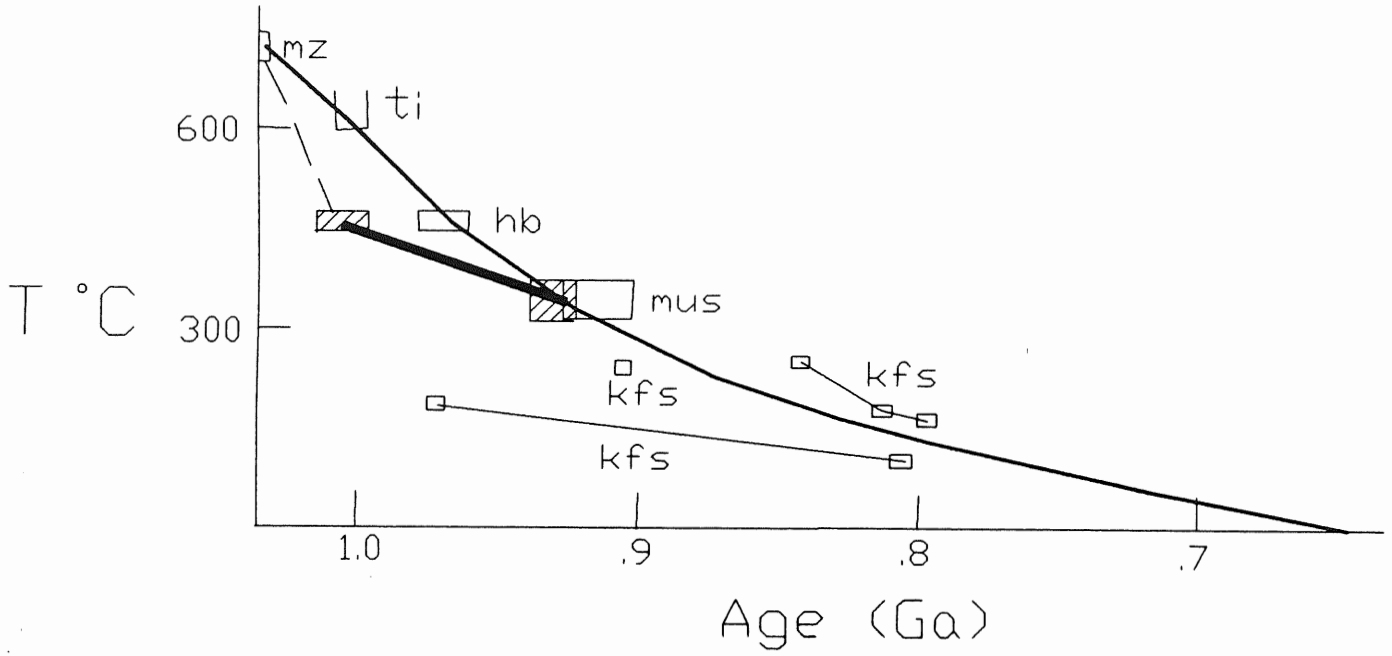

Figure 5.1. Cooling curve for the eastern end of the transect. The hachured boxes represent the range of temperatures and ages for the data from the present transect. Open boxes display the data obtained by Culshaw et al. (1991) except the monazite at far left obtained by Corrigan (1990). For the present transect the dashed line represents the cooling rate between 700 °C and 500 °C and the thick line represents the cooling rate between 500 °C and 350 °C.

Using titanite data, Corrigan (1990) estimated that the peak metamorphism of the Britt Domain at Key Harbour reached 700 - 800 °C at 8 - 10 Kbar at 1035 Ma. Cooling from 700 - 800 °C to the 500 ± 50 °C (Hanes 1991) blocking temperature took ~30 million years (The three Britt Domain hornblendes of this study have an average age of ~1005 Ma), implying a cooling rate of 5 - 11 °C/million years (Fig.5.1). Cooling from 500 ± 50 °C (Hanes 1991) to the 350 ± 50 °C closure temperature of the muscovite (Hanes 1991) took ~75 million years, implying a cooling rate of 1 - 4 °C/million years (Fig.5.1). Cosca et al. (1991) believe that the near-horizontal Cambrian-Ordovician strata unconformably overlying Grenville rocks in Ontario limit the latest age of surface exposure of the CGB and CMB to ~600 Ma. Applying the 600 Ma limit to the rocks in the present transect, the minimum cooling rate from the time of muscovite closure to the time when the rocks were exposed to the surface becomes 0.8 - 1.2 °C/million years (Fig.5.1), assuming a surface temperature of 20 °C. This result depends on the assumption that Cambrian-Ordovician strata extended over this transect.

The two eastern hornblende samples within the GFTZ (Locations 4 and 5) have similar ages to hornblendes from the present transect in the Britt domain. Although they have no muscovite pairs, it is likely that they underwent the same cooling history as the Britt domain rocks (Locations 6, 7, and 8).

The rocks containing the old age grouping of hornblendes in the west (Locations 1, 2, and 3) likely contain excess argon which artificially elevates the age values. The absence of reliable $^{40}Ar/^{39}Ar$ ages precludes the determination of a cooling history of these rocks.

The 5 - 11 °C/million years cooling rate from 700 - 800 °C to 500 ± 50°C in the eastern portion of the present transect is greater than the result of ~4 °C/million years for the Britt domain southeast of Key Harbour (Check 1989 and Culshaw et al. 1991) and the 2 - 4 °C/million years rate determined further south in the Parry Sound domain of the CGB (Cosca et al. 1991). Cooling between 600 °C and 300 °C in the area west of Beaverstone Bay proceeded at a very fast pace (Haggart 1991); far faster than the rate of 5 - 11 °C/million years in the eastern portion of the present transect.

Cooling between 500 ± 50 °C and ~350 ± 50 °C occurs at similar rates (1 - 4 °C/million years) in the CGB for the eastern portion of the present transect and the areas studied by Check (1989), Culshaw (1991) and Cosca (1991). Below ~300 °C the cooling in these areas slowed to ~1 °C/million years. The transect in the GFTZ studied by Haggart (1991) cooled rapidly until 300 Ma before adopting a rate of ~1 °C/million years.

In the transect studied by Haggart (1991), hornblende ages become younger and titanites become progressively more

reset towards the east, with the youngest hornblendes and most reset titanites residing near Beaverstone Bay. This pattern may be the result of a thermal event whose influence increased from west to east (Haggart 1991). A tectonically-driven rapid exhumation is the likely cause of the thermal event. Haggart (1991) explains the increasing ages to the west by shearing and folding of the thrust; the highest point of the antiformal thrust would contain rocks which were rapidly exhumed from great depth. Towards the west, the rocks at surface today would have suffered less rapid uplift and come from shallower depths. Because the most rapid uplift and exhumation occurred in the hanging wall above the shear zone, the most rapid cooling would occur there. The cooling rates seem to decrease towards the east away from Beaverstone Bay as well, determined by comparisons of the cooling rates calculated from the present transect and the transects studied by Check (1989), Culshaw et al. (1991), and Cosca et al. (1991).

The trend noted by Mckenzie et al. (1991) and Culshaw et al. (1991) for muscovite ages to become older to the northwest seems to continue in the present study area as far as the CGB/GFTZ boundary.

5.3 Tectonic Model

The average age of the five hornblendes in the eastern portion of the transect of this study (from within the eastern GFTZ to Dead Island) is higher than the uniform age of hornblendes across the transect by Check (1989) and Culshaw et al. (1991) (Fig 4.6). Northwest-directed thrusting cannot easily explain the rise in age from ~970 Ma hornblendes at Key Harbour to the ~1005 Ma hornblendes west of Dead Island. The data can be more easily explained by extension, so that as the structurally overlying southeast block (containing Key Harbour) slid down the former thrust fault towards the southeast, the depth to which the northwest block (containing the present transect) was buried became drastically reduced. The northwest block readjusted to a new geothermal gradient by rapid cooling, so that the hornblendes contained within it reached closure before those in the southeast block, which did not shed any overlying rock as a result of extension. Kinematic indicators to the east of Dead Island (east of the present transect) indicate topside-down movement of the crustal block containing Key Harbour (Culshaw pers. comm. 1992).

Notice in the cooling curve (Fig. 5.1) that the line drawn from the monazite to the hornblende represents fast cooling. The fast cooling rate makes sense if tectonic unroofing of the footwall block occurred. Note that this

curve is based on the assumption that the two crustal blocks shared the same thermal history prior to 1035 Ma, the age of peak metamorphism in the Key Harbour rocks.

The Grenvillian tectonics of the eastern portion of the GFTZ between Beaverstone Bay and the CGB boundary would be of great interest because of the contrasting tectonic styles of the areas immediately to the east and the west. The three westernmost hornblendes (and muscovite) of the present transect most likely suffered excess argon contamination, however, making the $^{40}Ar/^{39}Ar$ ages determined from these hornblendes unusable for tectonic interpretation.

CHAPTER 6: CONCLUSIONS

1) The three hornblendes in the CGB (Locations 6 - 8) and the two in the eastern portion of the GFTZ (Locations 4 and 5) do not seem to have suffered biotite contamination and have well behaved spectra which yield geologically reasonable $^{40}Ar/^{39}Ar$ ages ranging from 1016 - 995 Ma. The $^{40}Ar/^{39}Ar$ ages seem to represent true hornblende cooling ages.

2) The three hornblendes in the western GFTZ examined in this transect (Locations 1 - 3) do not seem to suffer biotite contamination and have well-behaved spectra. The age of this group of hornblendes is considerably higher than hornblendes to the west and east, however, and the ages within the group vary from 1028 Ma to 1120 Ma. In addition to the anomalously high hornblende ages the westernmost location contains a muscovite with a higher $^{40}Ar/^{39}Ar$ age than the hornblende. Excess argon likely artificially elevates the ages of these three hornblende samples, therefore they are not usable for thermal or tectonic calculations.

3) The trend for muscovites to become older to the north continues across the CGB to the boundary of the CGB/GFTZ.

4) The cooling rate at high temperatures (700 - 800 °C to 500 ± 50 °C) is very rapid in the western GFTZ near Beaverstone Bay (Haggart 1991). The cooling rate at high

temperature is less (5 - 11 °C/million years) in the western CGB of the present transect, and less again (2 - 4 °C/million years) east and south of Key Harbour (Check 1989, Culshaw et al. 1991, and Cosca et al. 1991). The cooling rate seems to become gradationally less towards the east away from Beaverstone Bay. The cooling rates below 300 °C in all areas along Georgian Bay are similar (~1 °C/million years).

5) The hornblende ages in the eastern part of this transect are older than those determined by Check (1989); Culshaw et al. (1991) in the western Britt Domain. This can be explained by extension, so that the area represented by the eastern portion of the present transect was the tectonically unroofed footwall.

6) No reliable thermochronological information exists between Beaverstone Bay and Location 4 of the present transect. It is doubtful whether further $^{40}Ar/^{39}Ar$ ages would be useful, since excess argon seems to contaminate hornblende and muscovite in the area. Thermochronological methods which rely on the radioactive decay of other elements would prove very useful in illuminating thermal and tectonic history in this area.

REFERENCES

Bowen R (1988) Isotopes in the earth sciences. Elsevier Applied Science Publishers Ltd

Check G (1989) $^{40}Ar/^{39}Ar$ Thermochronology of the Britt domain, Grenville province, Georgian Bay, Ontario. BSc Honours Thesis, Dalhousie University

Corrigan D (1990) Geology and U-Pb geochronology of the Key Harbour area, Britt domain, Southwest Grenville Province. MSc Thesis, Dalhousie University

Cosca MA, Sutter JF, Essene EJ (1991) Cooling and inferred uplift/erosion history of the Ontario Grenville Province: constraints from $^{40}Ar/^{39}Ar$ thermochronometry. Tectonics 10:959-977

Culshaw NG, Reynolds PH, Check G (1991). A $^{40}Ar/^{39}Ar$ study of post-tectonic cooling in the Britt domain of the Grenville Province, Ontario. E Plan Sci Letts 105:405-415

Dalrymple GB, Lanphere MA (1969) Potassium-argon dating: Principles, Techniques, and Applications to Geochronology. Freeman, San Francisco

Davidson A (1984). Identification of ductile shear zones in the southwestern Grenville Province of the Canadian Shield. In: Precambrian tectonics illustrated. Kröner A, Greiling R (eds) Schweizerbart'sche Verlagsbuchhandlung, Stuttgart, pp263-279

Davidson A (1985) Tectonic framework of the Grenville Province in Ontario and western Quebec, Canada. In: The deep Proterozoic crust in the North Atlantic provinces. Tobi AC, Touret LR (eds) D.Reidel Publishing Company, Dordrecht, pp133-149

Davidson A, Bethune KM (1988) Geology of the north shore of Georgian Bay, Grenville province of Ontario. GSC Paper 88-1C:135-144

Davidson A, Culshaw NG, Nadeau L (1982) A tectonometamorphic framework for part of the Grenville Province, Parry Sound region, Ontario. In: GSC Paper 82-1A:175-190

Davidson A, Nadeau L, Grant SM, Pryer LL (1985) Studies in the Grenville Province of Ontario. In: GSC Paper 85-1A:463-483

Dickin AP, McNutt RH (1989) Nd model age mapping of the southeast margin of the foreland in the Grenville Province of Ontario. Geology 17:299-302

Dodson MH (1973) Closure temperature in cooling geochronological and petrological systems. Contrib Mineral Petrol 40:259-274

Easton RM (1986) Geochronology of the Grenville Province. In The Grenville Province. Moore JM, Davidson A, Baer AJ (eds) Geol Assoc Can Spec Pap 31, pp123-173

Fahrig WF, West TD (1986) Diabase dyke swarms of the Canadian Shield. GSC, Map 1627A

Fleck RJ, Sutter JF, Elliot DH (1977) Interpretation of discordant $^{40}Ar/^{39}Ar$ age-spectra of Mesozoic tholeiites from Antarctica. Geochim Cosmochim Acta 41:15-32

Gariépy C, Verner D, Doig R. (1990) Dating Archean metamorphic minerals southeast of the Grenville Front, western Quebec, using Pb isotopes. Geology 18:1078-1081

Grasty RL, Mitchell JG (1966) Single sample potassium-argon ages using the omegatron. E Plan Sci Letts 1:121-122

Haggart MJ (1991) Thermal history of the Grenville Front Tectonic Zone, central Ontario. MSc Thesis, Dalhousie University

Hanes JA (1991) K-Ar and $^{40}Ar/^{39}Ar$ geochronology: methods and applications. In: Short course handbook on applications of radiogenic isotope systems to problems in geology. Mineralogical Association of Canada, pp27-57

Harrison TM (1990) Some observations on the interpretations of feldspar $^{40}Ar/^{39}Ar$ results. Chem Geol 80:219-229

Lee JKW, Onstott TC, Cashman KV, Cumbest RJ, Johnson D (1991) Incremental heating of hornblende in vacuo: Implications for 40Ar/39Ar geochronology and the interpretation of thermal histories. Geology 19:872-876

McDougall I, Harrison TM (1988) Geochronology and thermochronology by the $^{40}Ar/^{39}Ar$ method. Oxford University Press, New York

McKenzie KJ (1991) Muscovite $^{40}Ar/^{39}Ar$ geochronology of the western Parry Sound and Britt domains, Central Gneiss Belt, Grenville Province. BSc Honours Thesis, Dalhousie University

Merrihue C, Turner G (1966) Potassium-argon dating by activation with fast neutrons. J Geophys Res 71:2852-2857

Mitchell JG (1968) The $^{40}Ar/^{39}Ar$ method for potassium-argon age determination. Geochim Cosmochim Acta 3:781-790

Nunn GAG, Heaman LM, Krough TM (1990) U-Pb geochronological evidence for Archean crust in the continuation of the Rae Province (eastern Churchill Province), Grenville Front Tectonic Zone, Labrador. Geoscience Canada 17:259-264

Roddick JC, Cliff RA, Rex DC (1980) The evolution of excess argon in Alpine biotites - a $^{40}Ar/^{39}Ar$ analysis. E Plan Sci Letts 48:185-208

Turner G, Miller JA, Grasty RL (1966) The thermal history of the Bruderheim meteorite. E Plan Sci Letts 1:155-157

Wynne-Edwards HR (1972) The Grenville Province. In: Variations in tectonic styles in Canada. Price RA, Douglas RJW (eds) Geol Assoc Can Spec Pap 11, pp263-334

APPENDIX 1: THERMOCHRONOLOGICAL SUMMARIES

Appendix 1.1 Summaries from Hornblendes

ND-91B HORNBLENDE SUMMARY

°C	mV 39	% 39	AGE (Ma)	% ATM	37/39	36/40	39/40	% IIC
850	5	.7	6788.6 +/- 360.5	.5	2.15	.000019	.000048	.14
950	11.9	1.6	1467.9 +/- 13.3	2.9	2.69	.000098	.001583	.2
1000	110	15.3	1068.8 +/- 2.4	.8	3.1	.000029	.002513	.26
1025	192.5	26.9	1066.3 +/- 2.2	.2	3.14	.000009	.002536	.26
1050	128.5	17.9	1054.5 +/- 2.1	.3	3.2	.000012	.002571	.27
1075	226.5	31.6	1052.2 +/- 2	.1	3.16	.000004	.002585	.26
1100	11.4	1.5	1067.6 +/- 15.9	2.3	3.32	.000079	.002479	.27
1125	14.9	2	1046.5 +/- 15.1	2.4	3.22	.000083	.002542	.27
1200	13.6	1.9	1115 +/- 13.2	1.9	3.44	.000067	.002348	.28

TOTAL GAS AGE = 1337.1 Ma

J = .00205

ERROR ESTIMATES AT ONE SIGMA LEVEL

37/39,36/40 AND 39/40 Ar RATIOS ARE CORRECTED FOR INTERFERING ISOTOPES

% IIC - INTERFERING ISOTOPES CORRECTION

ND-94B HORNBLENDE SUMMARY

°C	mV 39	% 39	AGE (Ma)	% ATM	37/39	36/40	39/40	% IIC
750	12.5	3.1	529.2 +/- 4.3	8.5	3.27	.00029	.005495	.36
950	16.4	4.1	617.5 +/- 5.5	3.9	1.06	.000133	.004822	.1
1050	155.7	39.7	1115.8 +/- 2.3	.3	3.05	.00001	.002386	.25
1075	80.8	20.6	1127.7 +/- 3.1	.1	3.11	.000006	.002355	.25
1100	51.7	13.2	1116.5 +/- 3.4	.3	3.12	.000011	.002383	.25
1125	15.5	3.9	1131.8 +/- 9.4	1.2	3.39	.000041	.002319	.28
1150	12.6	3.2	1131.2 +/- 14.2	1.4	3.66	.000048	.002316	.3
1200	9.3	2.3	1074.4 +/- 10.6	2.2	3.79	.000076	.00246	.31
1250	18	4.6	1055.4 +/- 3.8	1.8	3.75	.000062	.00253	.31
1300	18.7	4.7	1030 +/- 8.4	3.3	4.02	.000113	.002572	.34

TOTAL GAS AGE = 1077.1 Ma

J = .00205

ERROR ESTIMATES AT ONE SIGMA LEVEL

37/39,36/40 AND 39/40 Ar RATIOS ARE CORRECTED FOR INTERFERING ISOTOPES

% IIC - INTERFERING ISOTOPES CORRECTION

ND-102C HORNBLENDE SUMMARY

°C	mV 39	% 39	AGE (Ma)	% ATM	37/39	36/40	39/40	% IIC
650	1.4	.1	2544 +/- 595.5	12.8	3.74	.000434	.000576	.26
750	3	.3	885.3 +/- 85.5	33.6	2.81	.001137	.002147	.25
850	1.8	.1	2065.6 +/- 142.7	10.9	1.93	.00037	.000851	.13
900	1.6	.1	1509.2 +/- 167.3	10.3	2.4	.000351	.001403	.18
950	6.6	.7	1274.6 +/- 20.1	4.5	2.76	.000152	.001905	.22
1000	45.4	4.8	1040.6 +/- 3.9	1.1	2.65	.000038	.002596	.22
1050	77.9	8.3	1027.7 +/- 2.1	.5	2.71	.000017	.002655	.23
1075	331.6	35.5	1027.4 +/- 1.9	.1	2.71	.000006	.002665	.23
1100	104.9	11.2	1029.3 +/- 2.7	.2	2.71	.000007	.002658	.23
1150	306.6	32.8	1028.4 +/- 2	.1	2.83	.000006	.002662	.24
1200	40.1	4.3	1030.6 +/- 3.7	2.2	3.08	.000076	.0026	.26
1250	8.4	.9	999.1 +/- 16.2	6.6	2.9	.000225	.002585	.24
1300	2.3	.2	1742.1 +/- 189.8	16.5	2.62	.00056	.001051	.19

TOTAL GAS AGE = 1039.5 Ma

J = .00205

ERROR ESTIMATES AT ONE SIGMA LEVEL

37/39,36/40 AND 39/40 Ar RATIOS ARE CORRECTED FOR INTERFERING ISOTOPES

% IIC - INTERFERING ISOTOPES CORRECTION

ND-103 HORNBLENDE SUMMARY

°C	mV 39	% 39	AGE (Ma)	% ATM	37/39	36/40	39/40	% IIC
750	9.2	1.3	1510.5 +/- 25.3	6.2	3.81	.000211	.001466	.29
950	9	1.3	1086.6 +/- 9.8	4.9	1.54	.000168	.002356	.12
1050	111	16.4	1009.1 +/- 2.1	.7	2.77	.000026	.002712	.23
1075	81.6	12.1	996 +/- 2.5	.6	2.82	.000022	.002762	.24
1100	100.9	14.9	998 +/- 2.1	.2	2.82	.000008	.002767	.24
1125	106.7	15.8	994.6 +/- 2.3	.3	2.82	.000012	.002776	.24
1150	71.3	10.5	995 +/- 2.4	.9	2.94	.000032	.002758	.25
1175	43.7	6.4	995 +/- 2.8	.5	2.91	.000019	.002768	.25
1200	16.5	2.4	1014.7 +/- 9	1.2	3.04	.000042	.00268	.26
1250	58.1	8.6	997.9 +/- 3.1	.6	2.96	.00002	.002757	.25
1300	32.7	4.8	1013.5 +/- 5.4	2.4	2.92	.000082	.002653	.25
1350	32.6	4.8	1013.9 +/- 4.9	3.8	2.87	.000132	.002611	.24

TOTAL GAS AGE = 1009.8 Ma

J = .00205

ERROR ESTIMATES AT ONE SIGMA LEVEL

37/39,36/40 AND 39/40 Ar RATIOS ARE CORRECTED FOR INTERFERING ISOTOPES

% IIC - INTERFERING ISOTOPES CORRECTION

ND-33 HORNBLENDE SUMMARY

°C	mV 39	% 39	AGE (Ma)	% ATM	37/39	36/40	39/40	% IIC
750	1.1	.3	879.6 +/- 199.6	22.4	3.39	.00076	.002529	.3
950	3	1	1080.9 +/- 52.5	6.2	1.83	.00021	.002342	.15
1050	31.6	10.7	1017.2 +/- 4.7	.9	2.89	.00003	.002681	.24
1075	29.6	10.1	1002.1 +/- 6.7	.7	2.98	.000024	.002739	.25
1100	93.2	31.8	1006.6 +/- 3.9	.3	3.27	.000011	.002734	.28
1125	53.7	18.3	993.8 +/- 3	.6	3.08	.000023	.00277	.26
1150	24.3	8.3	984.9 +/- 6.3	2.5	3.13	.000084	.002751	.27
1200	20.2	6.8	994.9 +/- 4.6	.9	3.26	.00003	.002759	.28
1250	36	12.2	1001.9 +/- 4.7	.9	3.15	.000031	.002734	.27

TOTAL GAS AGE = 1002.1 Ma

J = .00205

ERROR ESTIMATES AT ONE SIGMA LEVEL

37/39,36/40 AND 39/40 Ar RATIOS ARE CORRECTED FOR INTERFERING ISOTOPES

% IIC - INTERFERING ISOTOPES CORRECTION

ND-38A HORNBLENDE SUMMARY

°C	mV 39	% 39	AGE (Ma)	% ATM	37/39	36/40	39/40	% IIC
950	11.1	2.8	841.3 +/- 16.7	5.2	1.62	.000178	.003267	.14
1050	53.7	13.9	1000.9 +/- 3.4	1	4.96	.000034	.002735	.42
1075	55.3	14.3	1002.9 +/- 2.7	.4	4.93	.000014	.002745	.42
1100	149.7	38.7	1017.1 +/- 2.2	.1	4.67	.000006	.002701	.39
1125	53.6	13.8	1016.3 +/- 4.3	17.2	4.59	.000583	.002241	.39
1150	23.9	6.2	1007.4 +/- 8.1	1.6	4.71	.000054	.002696	.4
1175	25.9	6.7	1021 +/- 6.1	2.3	4.86	.00008	.002629	.41
1200	12.8	3.3	1004.2 +/- 10.1	3.1	5.06	.000108	.002663	.43

TOTAL GAS AGE = 1007.1 Ma

J = .00205

ERROR ESTIMATES AT ONE SIGMA LEVEL

37/39,36/40 AND 39/40 Ar RATIOS ARE CORRECTED FOR INTERFERING ISOTOPES

% IIC - INTERFERING ISOTOPES CORRECTION

ND-49C HORNBLENDE SUMMARY

°C	mV 39	% 39	AGE (Ma)	% ATM	37/39	36/40	39/40	% IIC
750	1.3	.4	1514.5 +/- 145	14.9	8.57	.000505	.001325	.65
950	2.2	.6	1155 +/- 78.1	12.6	4.13	.000428	.001995	.34
1050	82.7	25	1017.1 +/- 2.5	.8	3.63	.000028	.002683	.31
1075	60.9	18.4	1008 +/- 3.8	.5	3.68	.000019	.002722	.31
1100	76.9	23.3	1004 +/- 2.3	.4	3.65	.000015	.002739	.31
1125	65.2	19.7	1009 +/- 3	.4	3.65	.000015	.002721	.31
1150	13.6	4.1	1012.6 +/- 14.6	3	4.17	.000104	.002638	.35
1200	12.6	3.8	999.2 +/- 10.5	2.1	4.99	.000071	.00271	.42
1250	14.2	4.3	1008.5 +/- 9.1	3.4	4.67	.000116	.002642	.39

TOTAL GAS AGE = 1012.9 Ma

J = .00205

ERROR ESTIMATES AT ONE SIGMA LEVEL

37/39,36/40 AND 39/40 Ar RATIOS ARE CORRECTED FOR INTERFERING ISOTOPES

% IIC - INTERFERING ISOTOPES CORRECTION

ND-107A HORNBLENDE SUMMARY

°C	mV 39	% 39	AGE (Ma)	% ATM	37/39	36/40	39/40	% IIC
850	8	1.3	1091.9 +/- 19	9.6	1.12	.000326	.002226	.09
950	31.8	5.5	1026.6 +/- 6.2	1.8	2.3	.000064	.002622	.19
1000	131.3	22.7	996 +/- 4.2	.4	3	.000013	.002769	.25
1025	112.7	19.4	994.2 +/- 3.8	.3	2.98	.000011	.002778	.25
1050	197.3	34.1	994.1 +/- 3.8	.2	2.96	.000007	.002781	.25
1075	72.7	12.5	994.7 +/- 3.9	.2	2.87	.000007	.002779	.24
1100	13.6	2.3	1029.4 +/- 15	1	2.78	.000037	.002634	.23
1150	10.6	1.8	1009.5 +/- 12.1	1.7	2.8	.00006	.002683	.24

TOTAL GAS AGE = 999 Ma

J = .00205

ERROR ESTIMATES AT ONE SIGMA LEVEL

37/39,36/40 AND 39/40 Ar RATIOS ARE CORRECTED FOR INTERFERING ISOTOPES

% IIC - INTERFERING ISOTOPES CORRECTION

Appendix 1.2 Summaries from Muscovites

ND-91C MUSCOVITE SUMMARY

°C	mV 39	% 39	AGE (Ma)	% ATM	37/39	36/40	39/40	% IIC
650	4.2	1.9	1147.5 +/- 38.4	9.6	.23	.000327	.002082	.01
800	48.2	21.6	1134.5 +/- 3.2	1.6	.02	.000055	.002302	0
900	131.6	59	1110.7 +/- 2.6	.4	.01	.000015	.002397	0
1000	14	6.2	1126.1 +/- 11.3	4.3	.04	.000148	.002261	0
1100	23.7	10.6	1107.5 +/- 6.2	2.1	.05	.000073	.002365	0
1200	1.1	.4	1166.1 +/- 167	30.7	1.23	.001039	.001562	.1

TOTAL GAS AGE = 1117.5 Ma

J = .00205

ERROR ESTIMATES AT ONE SIGMA LEVEL

37/39,36/40 AND 39/40 Ar RATIOS ARE CORRECTED FOR INTERFERING ISOTOPES

% IIC - INTERFERING ISOTOPES CORRECTION

ND-38B MUSCOVITE SUMMARY

°C	mV 39	% 39	AGE (Ma)	% ATM	37/39	36/40	39/40	% IIC
650	9.6	.4	891.1 +/- 12.8	10.4	.12	.000355	.002871	.01
750	26.9	1.2	938.6 +/- 6.1	10.7	.01	.000364	.002679	0
800	79.6	3.7	940.9 +/- 2.2	2.9	0	.0001	.002904	0
850	467	22.2	929.8 +/- 1.8	.4	0	.000013	.003027	0
875	312.2	14.8	929.4 +/- 1.8	.1	0	.000004	.003036	0
900	162.4	7.7	933.6 +/- 1.9	.2	0	.000007	.003017	0
925	157.6	7.5	932.8 +/- 1.9	.2	0	.000009	.003018	0
950	85.2	4	932 +/- 2.4	.3	0	.000012	.003019	0
975	130.6	6.2	930.6 +/- 2	.3	0	.00001	.003026	0
1000	196.6	9.3	930.1 +/- 2	.2	0	.000007	.003031	0
1025	176.9	8.4	925.7 +/- 2	.1	0	.000006	.003051	0
1050	174.2	8.3	928 +/- 1.9	.2	0	.000007	.00304	0
1075	68.8	3.2	928.1 +/- 2.6	.4	0	.000014	.003033	0
1100	36.3	1.7	955.7 +/- 2.9	1.1	0	.00004	.002898	0
1150	7.4	.3	997.4 +/- 24.3	6.3	.01	.000214	.0026	0
1200	6.8	.3	908.6 +/- 21.9	13.5	.02	.000457	.002707	0

TOTAL GAS AGE = 930.9 Ma

J = .00205

ERROR ESTIMATES AT ONE SIGMA LEVEL

37/39,36/40 AND 39/40 Ar RATIOS ARE CORRECTED FOR INTERFERING ISOTOPES

% IIC - INTERFERING ISOTOPES CORRECTION

ND-49F MUSCOVITE SUMMARY

°C	mV 39	% 39	AGE (Ma)	% ATM	37/39	36/40	39/40	% IIC
650	8.4	.3	1857.9 +/- 81.2	4.8	.16	.000163	.001083	.01
700	14.1	.6	933.9 +/- 5.3	16	.03	.000542	.002537	0
750	26	1.1	926.9 +/- 6	6.5	0	.000223	.00285	0
800	74.7	3.3	937 +/- 2.8	2.3	0	.00008	.002937	0
825	77.7	3.4	931.7 +/- 2.5	.4	0	.000015	.003017	0
850	967	42.8	932.4 +/- 1.9	.4	0	.000014	.003016	0
875	254	11.2	931.8 +/- 2	.1	0	.000004	.003026	0
900	182	8	931.6 +/- 1.9	.1	0	.000005	.003027	0
950	162.6	7.2	933.7 +/- 1.9	.1	0	.000005	.003017	0
1000	151.7	6.7	931.5 +/- 2.2	.1	0	.000005	.003026	0
1050	312.1	13.8	932.7 +/- 1.8	0	0	.000002	.003024	0
1150	20.6	.9	941 +/- 6.2	2.3	0	.000081	.002921	0
1200	6	.2	979.7 +/- 27.1	14.5	.01	.000493	.002427	0

TOTAL GAS AGE = 937.1 Ma

J = .00205

ERROR ESTIMATES AT ONE SIGMA LEVEL

37/39,36/40 AND 39/40 Ar RATIOS ARE CORRECTED FOR INTERFERING ISOTOPES

% IIC - INTERFERING ISOTOPES CORRECTION

ND-107B MUSCOVITE SUMMARY

°C	mV 39	% 39	AGE (Ma)	% ATM	37/39	36/40	39/40	% IIC
700	47	1.8	632.2 +/- 2.6	24.3	.16	.000825	.003693	.01
750	20.8	.8	963.6 +/- 6.2	12.6	.02	.000427	.002536	0
800	165.4	6.4	917.9 +/- 2.1	7.1	0	.000243	.002867	0
850	205.5	8	927.9 +/- 2	1.9	0	.000065	.002988	0
875	195.2	7.6	934.3 +/- 2	.8	0	.000029	.002994	0
900	234.5	9.1	933.1 +/- 1.8	.4	0	.000013	.003013	0
925	245	9.5	936 +/- 1.9	.3	0	.00001	.003004	0
950	93.1	3.6	928.2 +/- 2.7	.5	0	.000019	.003028	0
975	146.4	5.7	924.5 +/- 2.1	.4	0	.000015	.003047	0
1000	134.6	5.2	926.9 +/- 2	.4	0	.000014	.003038	0
1025	189.5	7.3	929.5 +/- 1.8	.4	0	.000015	.003026	0
1050	246.5	9.6	929.5 +/- 1.8	.3	0	.000011	.00303	0
1075	213.8	8.3	934.6 +/- 1.9	.1	0	.000006	.003013	0
1100	207.5	8.1	933.9 +/- 2.1	.2	0	.000007	.003015	0
1125	101.8	3.9	935.1 +/- 2.3	.3	0	.000011	.003007	0
1150	71.9	2.8	940.1 +/- 2.3	1	0	.000034	.002965	0
1200	38.8	1.5	1004.7 +/- 6.3	4.2	.01	.000145	.002631	0
1250	3.9	.1	760.3 +/- 126.4	54.7	.02	.001853	.001768	0

TOTAL GAS AGE = 927 Ma

J = .00205

ERROR ESTIMATES AT ONE SIGMA LEVEL

37/39,36/40 AND 39/40 Ar RATIOS ARE CORRECTED FOR INTERFERING ISOTOPES

% IIC - INTERFERING ISOTOPES CORRECTION

APPENDIX 2: INVERSE ISOCHRONS

The top diagram of each page is a wide-view graph whose axis begin at the origin. The small rectangle drawn around the data on the top graph is enlarged in the bottom graph. For explanation of inverse isochrons, see section 2.5

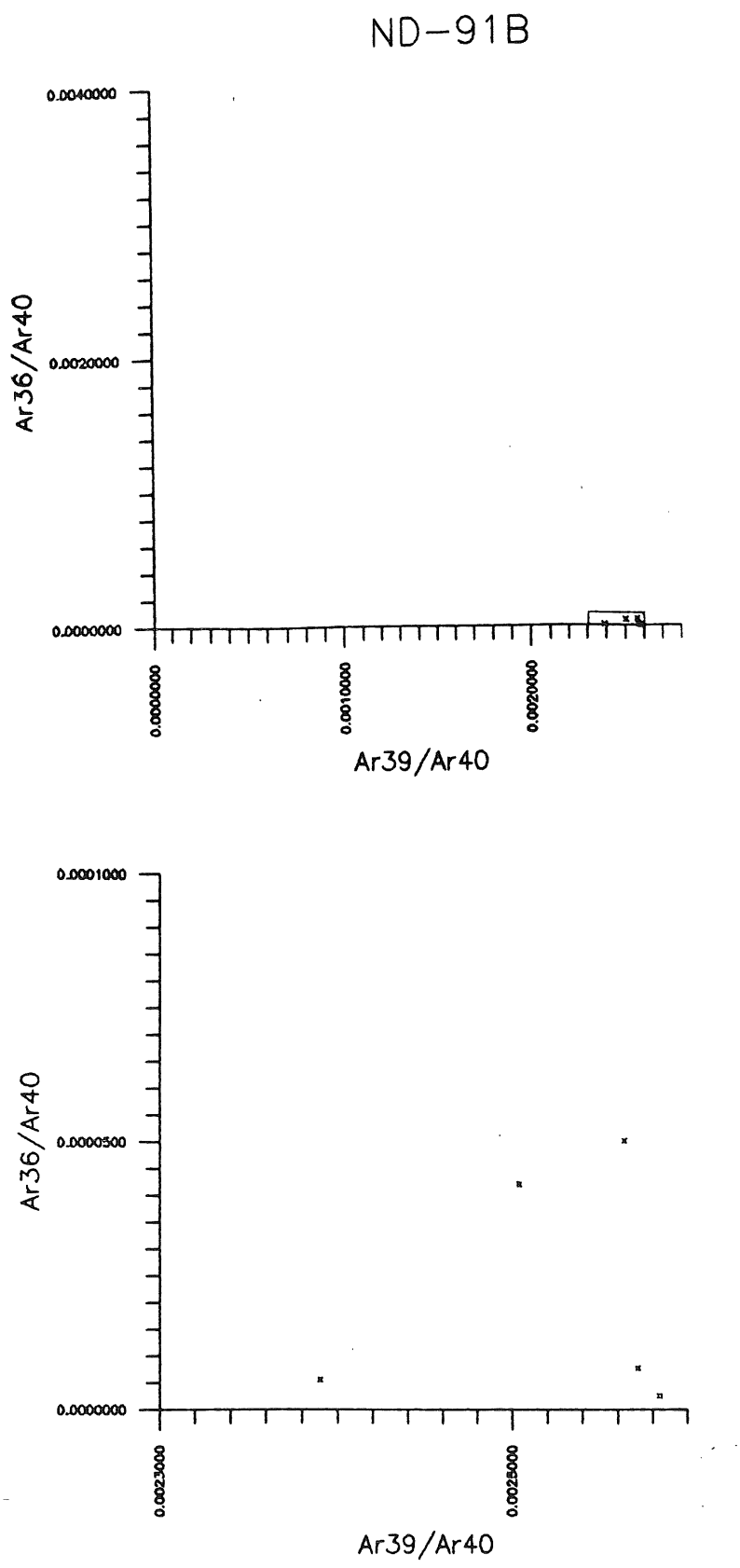

Appendix 2: Inverse Isochrons

ND-94B

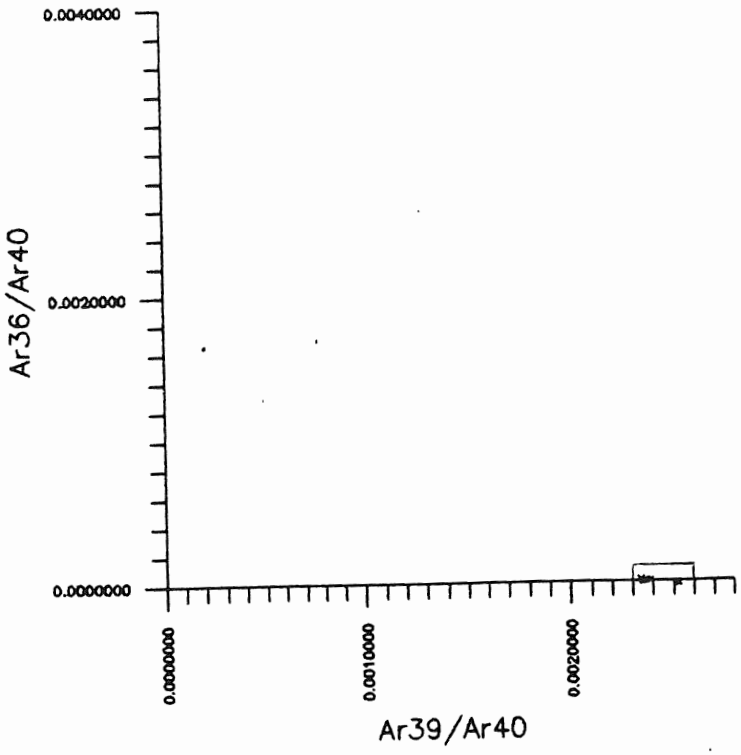

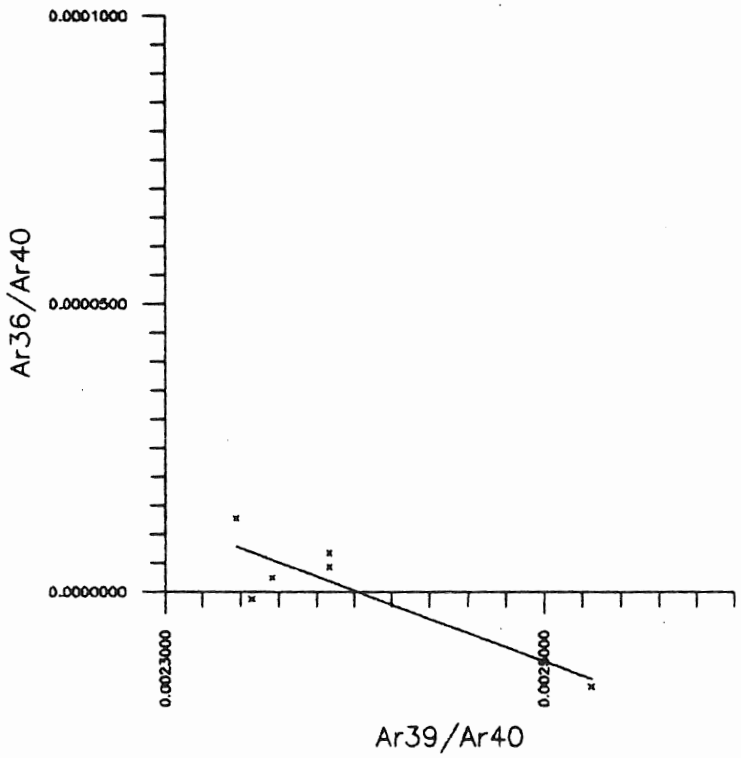

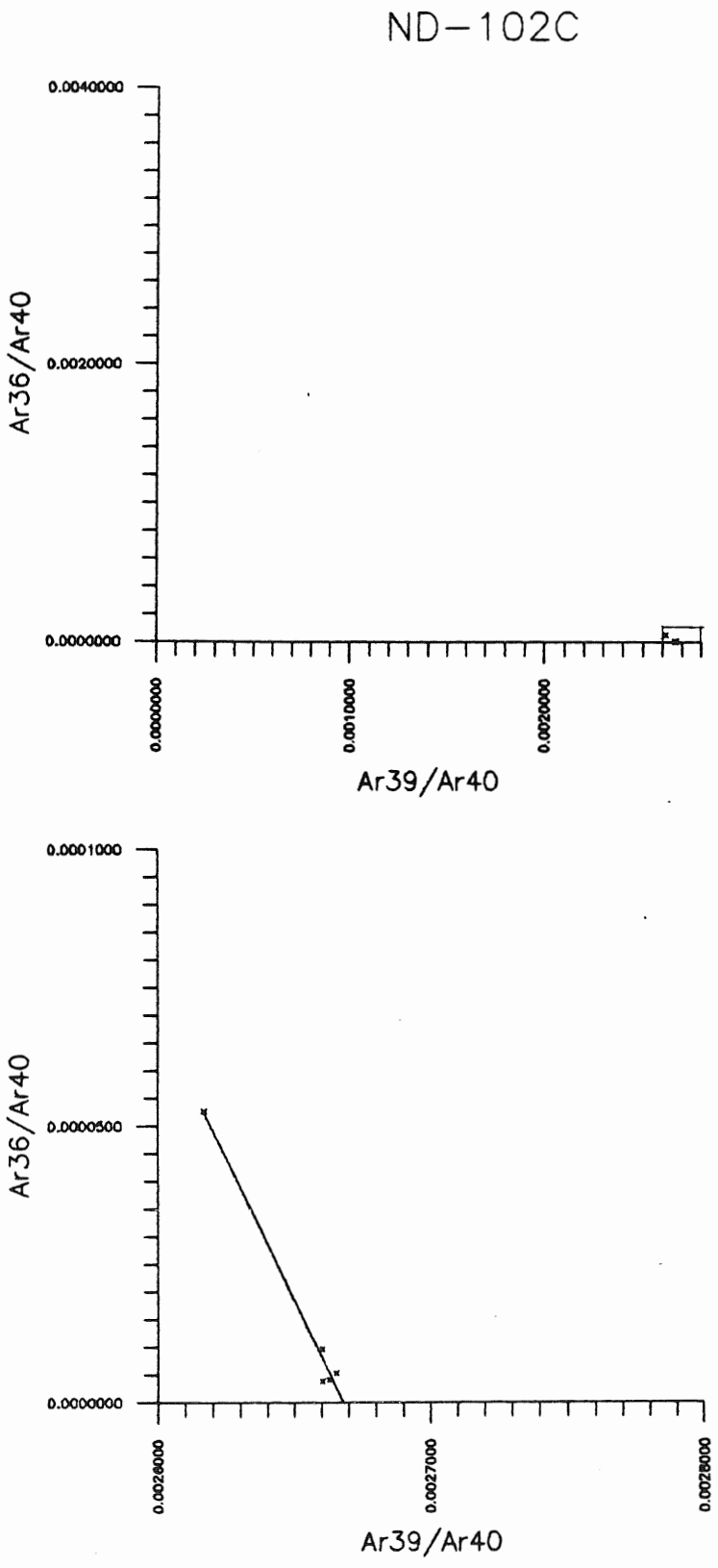
ND-102C
0.0040000
0.0020000
0.0000000
Ar36/Ar40
0.0000000
0.0010000
0.0020000
Ar39/Ar40
0.0001000
0.0000500
0.0000000
Ar36/Ar40
0.0026000
0.0027000
0.0028000
Ar39/Ar40

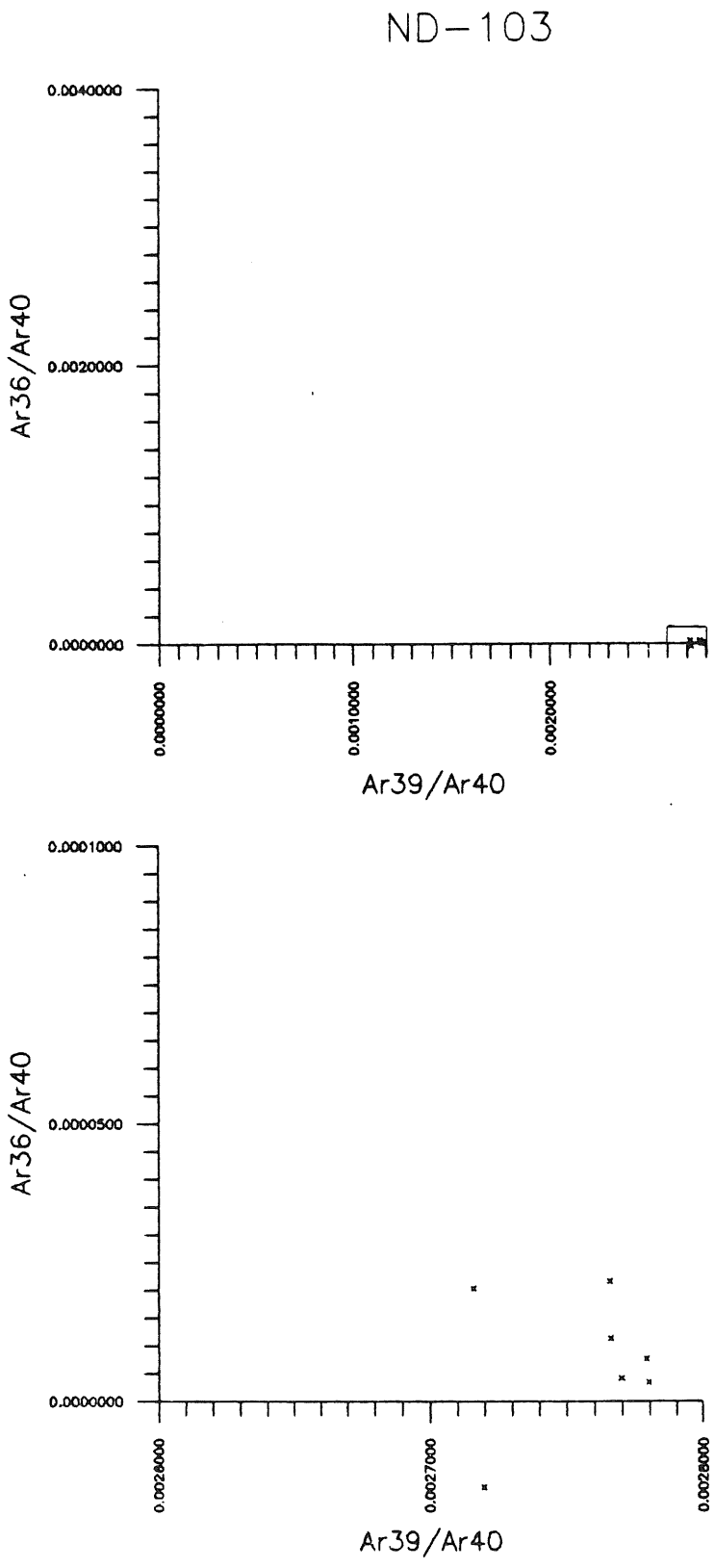
ND-103
0.0040000
0.0020000
0.0000000
Ar36/Ar40
0.0000000
0.0010000
0.0020000
Ar39/Ar40
0.0001000
0.0000500
0.0000000
Ar36/Ar40
0.0026000
0.0027000
0.0028000
Ar39/Ar40

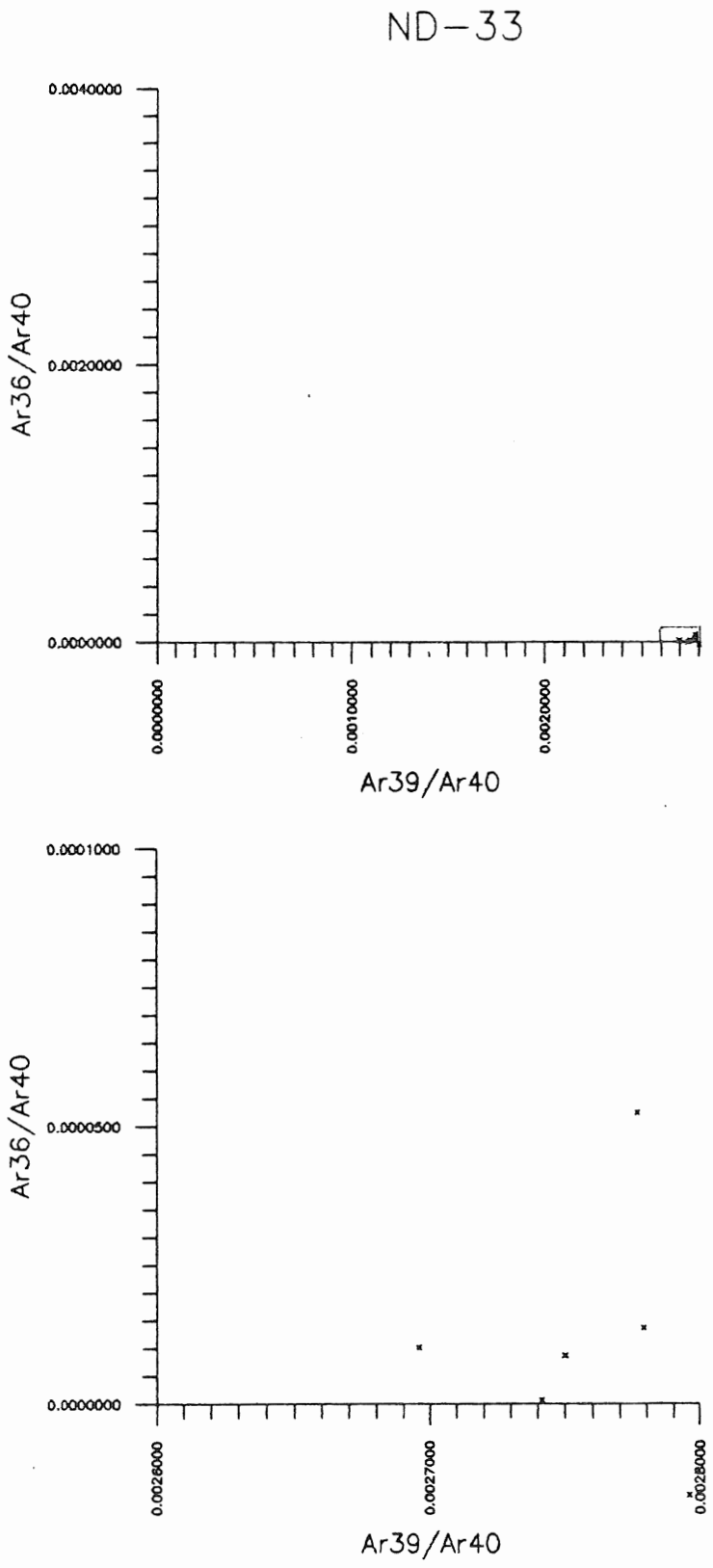
ND-33
0.0040000
0.0020000
0.0000000
Ar36/Ar40
0.0000000
0.0010000
0.0020000
Ar39/Ar40
0.0001000
0.0000500
0.0000000
Ar36/Ar40
0.0026000
0.0027000
0.0028000
Ar39/Ar40

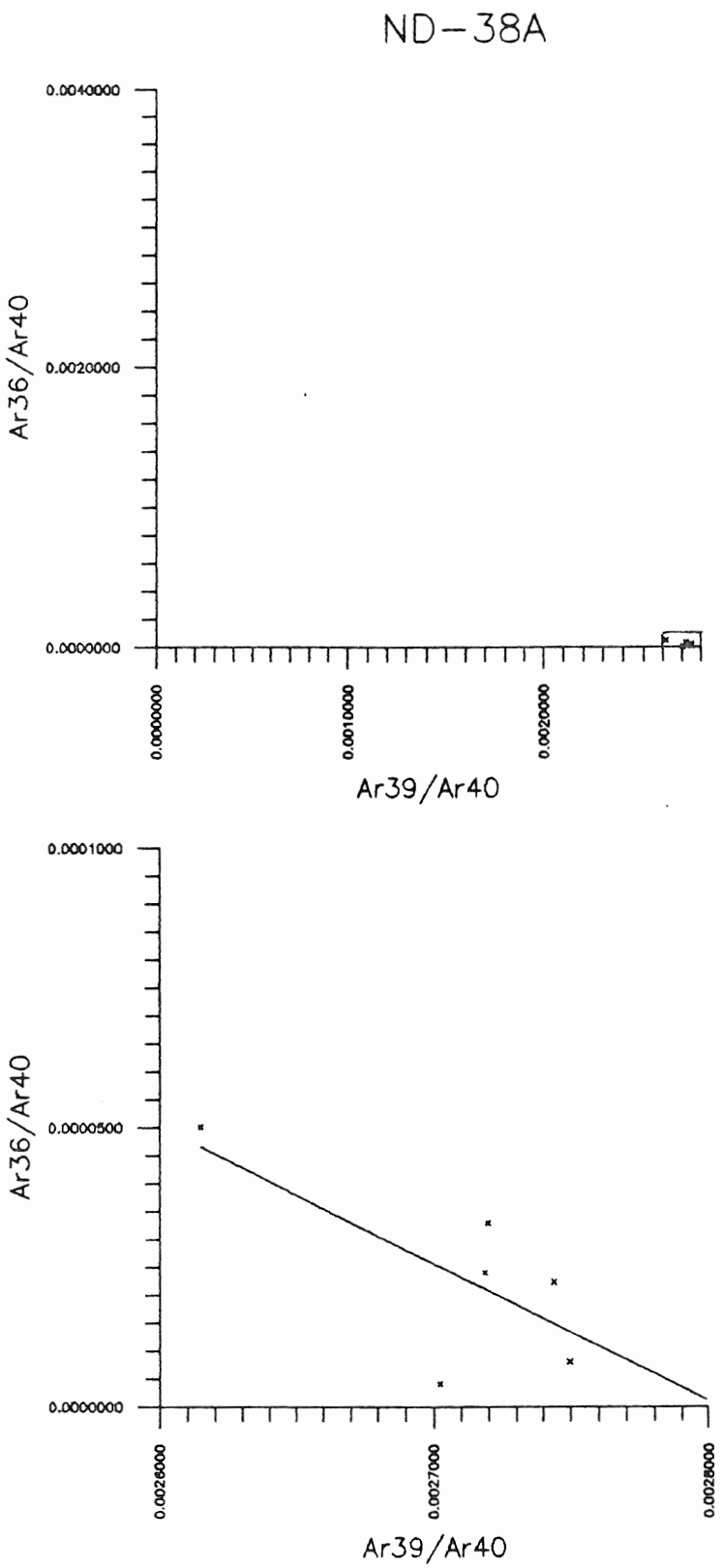
ND-38A
0.0040000
0.0020000
0.0000000
Ar36/Ar40
0.0000000
0.0010000
0.0020000
Ar39/Ar40
0.0001000
0.0000500
0.0000000
Ar36/Ar40
0.0026000
0.0027000
0.0028000
Ar39/Ar40

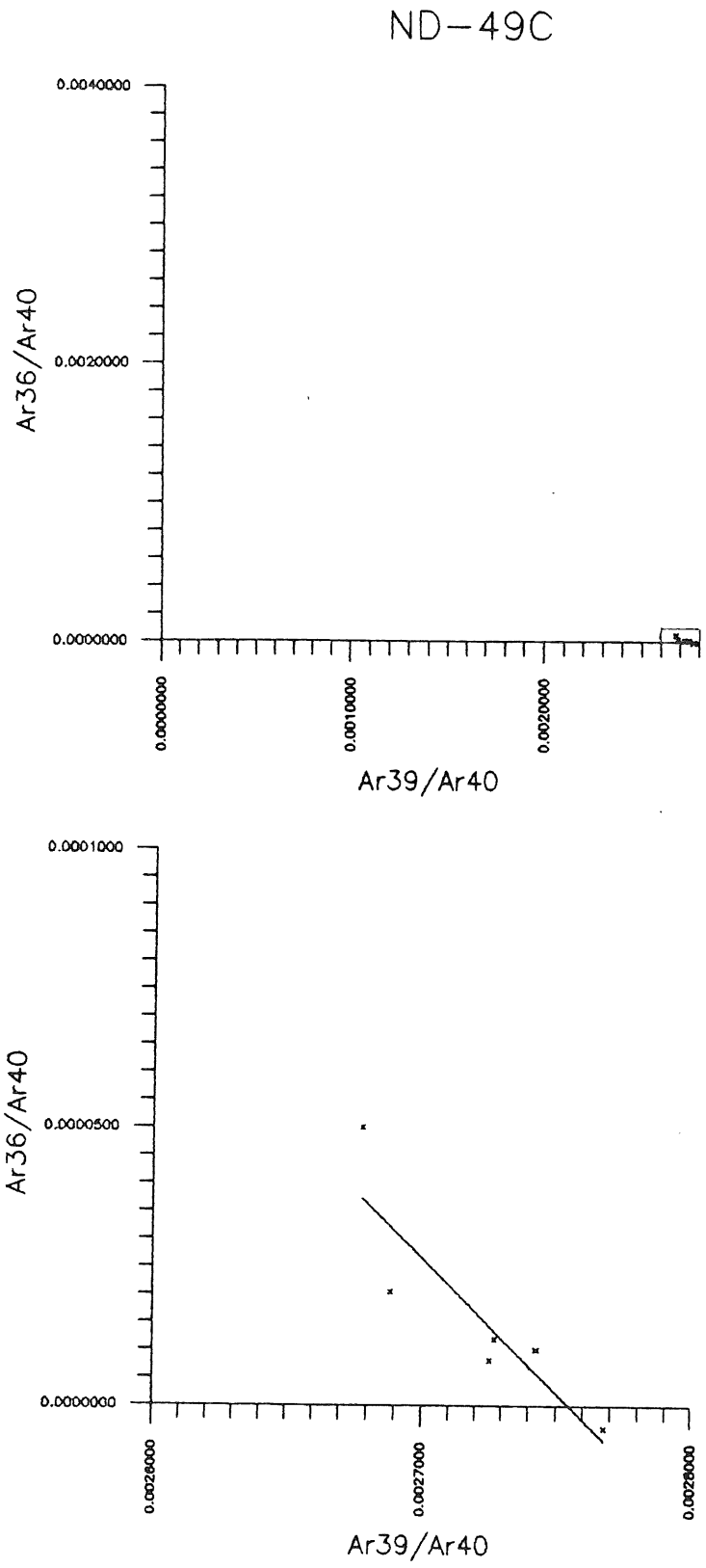
ND-49C
0.0040000
0.0020000
0.0000000
Ar36/Ar40
0.0000000
0.0010000
0.0020000
Ar39/Ar40
0.0001000
0.0000500
0.0000000
Ar36/Ar40
0.0026000
0.0027000
0.0028000
Ar39/Ar40

ND-107

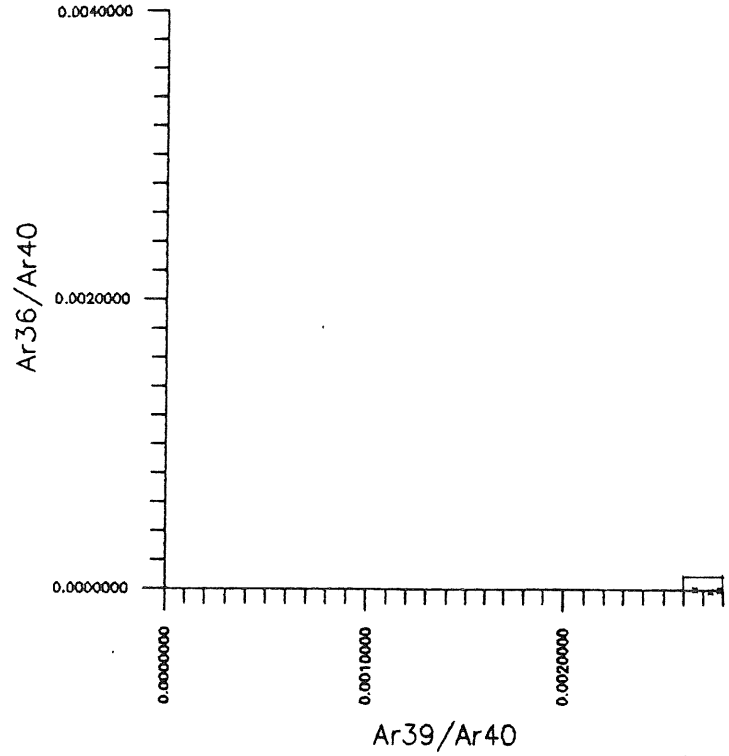
0.0040000
0.0020000
0.0000000
Ar36/Ar40
0.0000000
0.0010000
0.0020000
Ar39/Ar40

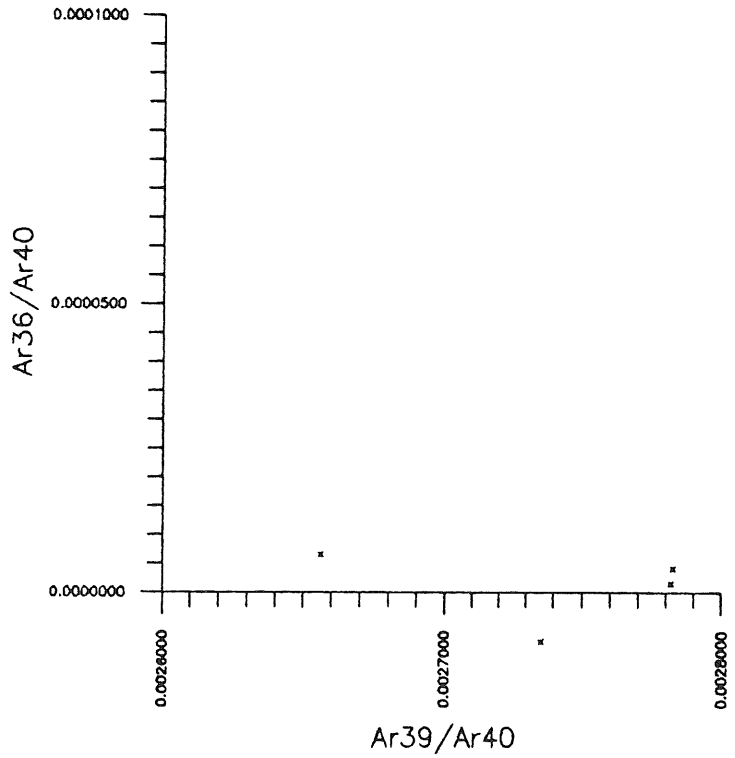
0.0001000
0.0000500
0.0000000
Ar36/Ar40
0.0026000
0.0027000
0.0028000
Ar39/Ar40

APPENDIX 3: MICROPROBE SUMMARY

Appendix 3.1. K_2O-Content of Hornblendes.

	Nd-91B			
	1	2	3	Av.
SiO2	42.136	42.138	42.140	42.138
TiO2	1.891	1.801	1.920	1.871
Al2O3	11.534	11.531	11.163	11.409
FeO	17.618	17.420	17.337	17.458
MnO	0.396	0.333	0.427	0.385
MgO	10.404	10.548	10.716	10.556
CaO	11.762	11.711	11.744	11.739
Na2O	1.854	2.008	1.776	1.879
K2O	1.598	1.551	1.488	1.546
Cr2O3				
BaO				
NiO				
TOTAL	99.193	99.042	98.711	98.982

	Nd-94B			
	1	2	3	Av.
SiO2	42.218	41.103	41.515	41.612
TiO2	2.088	2.224	2.096	2.136
Al2O3	11.168	11.093	10.956	11.072
FeO	21.642	21.643	21.767	21.684
MnO	0.679	0.535	0.516	0.577
MgO	8.088	7.956	8.052	8.032
CaO	11.092	10.742	11.011	10.948
Na2O	2.250	2.203	2.165	2.206
K2O	1.436	1.545	1.521	1.501
Cr2O3				
BaO				
NiO				
TOTAL	99.661	99.045	99.598	99.435

	Nd-102C		
	1	2	Av.
SiO2	41.448	41.764	41.606
TiO2	1.750	1.858	1.804
Al2O3	10.413	10.880	10.647
FeO	20.505	20.925	20.715
MnO	0.464	0.266	0.365
MgO	9.258	9.051	9.155
CaO	10.745	11.054	10.900
Na2O	2.468	2.469	2.469
K2O	1.580	1.697	1.639
Cr2O3	0.170	0.125	0.148
BaO			
NiO			
TOTAL	98.80	06.088	99.446

K2O-content of hornblendes (cont.)

Nd-103

	1	2	3	4	Av.
SiO2	41.437	41.895	41.944	42.158	41.859
TiO2	1.723	1.637	1.844	2.028	1.808
Al2O3	10.119	9.914	10.001	10.078	10.028
FeO	21.210	21.030	21.524	21.096	21.215
MnO	0.673	0.678	0.773	0.836	0.740
MgO	8.466	8.792	8.878	8.689	8.706
CaO	10.695	10.741	10.669	10.942	10.762
Na2O	2.398	2.252	2.445	2.328	2.356
K2O	1.566	1.494	1.533	1.533	1.532
Cr2O3					
BaO					
NiO					
TOTAL	98.287	98.433	99.610	99.688	99.005

Nd-33

	1	2	3	Av.
SiO2	42.355	42.270	41.731	42.119
TiO2	1.622	1.438	1.837	1.632
Al2O3	10.019	9.951	9.962	9.977
FeO	20.667	20.691	21.286	20.881
MnO	0.942	0.810	0.807	0.853
MgO	8.909	9.057	8.653	8.873
CaO	10.709	10.752	10.748	10.736
Na2O	2.334	2.215	2.367	2.305
K2O	1.449	1.305	1.476	1.410
Cr2O3				
BaO	0.221			
NiO	0.149			
TOTAL	99.375	98.490	98.866	98.910

Nd-38A

	1	2	3	4	5	Av.
SiO2	41.938	42.200	41.589	41.873	42.601	42.040
TiO2	1.814	1.644	1.730	1.158	1.464	1.562
Al2O3	12.876	12.796	12.945	12.930	12.099	12.729
FeO	15.745	15.877	16.455	16.775	17.084	16.387
MnO	0.211	0.198	0.313	0.241	0.389	0.270
MgO	11.149	10.997	10.583	10.872	10.967	10.914
CaO	11.998	11.940	11.861	11.695	11.969	11.893
Na2O	1.639	1.514	1.627	1.816	1.573	1.634
K2O	1.199	1.211	1.165	1.106	0.948	1.126
Cr2O3			0.098			
BaO						
NiO						
TOTAL	98.569	98.475	98.269	98.466	99.094	98.575

K2O-content of hornblendes (cont.)

	Nd-49C						
	1	2	3	4	5	6	Av.
SiO2	41.357	42.100	40.557	41.229	41.346	41.384	41.329
TiO2	2.162	1.701	1.818	2.314	1.837	1.865	1.950
Al2O3	11.814	11.493	11.455	11.729	11.716	11.772	11.663
FeO	19.474	19.149	19.399	19.439	19.700	19.571	19.455
MnO	0.112		0.177		0.180	0.154	0.104
MgO	9.241	9.635	9.322	9.244	9.150	9.428	9.337
CaO	11.280	11.373	10.852	11.181	11.085	11.179	11.158
Na2O	2.027	1.874	1.809	1.892	1.977	2.087	1.944
K2O	1.311	1.178	1.085	1.232	1.333	1.311	1.242
Cr2O3				0.089	0.093	0.099	
BaO					0.230		
NiO							
TOTAL	98.778	98.503	96.475	98.349	98.647	98.848	98.267

	Nd-107A			
	1	2	3	Av.
SiO2	42.011	41.257	41.028	41.432
TiO2	1.329	1.354	1.371	1.351
Al2O3	11.589	11.776	12.124	11.830
FeO	18.850	18.857	18.520	18.742
MnO	0.396	0.335	0.383	0.371
MgO	9.936	10.184	9.768	9.963
CaO	11.698	10.812	11.607	11.372
Na2O	1.970	1.750	1.967	1.896
K2O	1.640	1.555	1.624	1.606
Cr2O3		0.099		
BaO	0.158			
NiO				
TOTAL	99.577	97.979	98.392	98.649

Appendix 3.2. K-Content of Hornblendes

	Nd-91B			
	1	2	3	Av.
Si	19.697	19.698	19.699	19.698
Ti	1.134	1.801	1.151	1.362
Al	6.104	6.103	5.908	6.038
Fe	13.695	13.541	13.476	13.571
Mn	0.307	0.258	0.331	0.299
Mg	6.275	6.362	6.463	6.367
Ca	8.406	8.370	8.394	8.390
Na	1.375	1.490	1.317	1.394
K	1.327	1.288	1.235	1.283
Cr				
Ba				
Ni				
O	40.874	40.854	40.737	40.822
TOTAL	99.193	99.042	98.711	98.982

	Nd-94B			
	1	2	3	Av.
Si	19.268	19.214	19.407	19.296
Ti	1.252	1.330	1.257	1.280
Al	5.910	5.870	5.797	5.859
Fe	16.823	16.824	16.920	16.856
Mn	0.526	0.415	0.400	0.447
Mg	4.878	4.798	4.856	4.844
Ca	7.927	7.677	7.870	7.825
Na	1.669	1.634	1.606	1.636
K	1.192	1.283	1.263	1.246
Cr				
Ba				
Ni				
O	40.216	39.996	40.223	40.145
TOTAL	99.661	99.045	99.598	99.435

	Nd-102C		
	1	2	Av.
Si	19.376	19.523	19.450
Ti	1.049	1.114	1.082
Al	5.511	5.758	5.635
Fe	15.939	16.265	16.102
Mn	0.360	0.206	0.283
Mg	5.583	5.458	5.521
Ca	7.680	7.900	7.790
Na	1.831	1.832	1.832
K	1.312	1.409	1.361
Cr	0.117	0.085	0.101
Ba			
Ni			
O	40.047	40.538	40.293
TOTAL	98.803	100.088	99.446

K-content of hornblendes (cont.)

Nd-103

	1	2	3	4	Av.
Si	19.370	19.585	19.607	19.707	19.567
Ti	1.033	0.981	1.105	1.216	1.084
Al	5.355	5.247	5.293	5.334	5.307
Fe	16.487	16.347	16.731	16.399	16.491
Mn	0.521	0.525	0.599	0.648	0.573
Mg	5.106	5.302	5.354	5.240	5.251
Ca	7.644	7.676	7.625	7.820	7.691
Na	1.779	1.671	1.814	1.727	1.748
K	1.300	1.240	1.273	1.273	1.272
Cr					
Ba					
Ni					
O	39.692	39.859	40.210	40.326	40.022
TOTAL	98.287	98.433	99.610	99.688	99.005

Nd-33

	1	2	3	Av.
Si	19.800	19.760	19.508	19.689
Ti	0.973	0.862	1.101	0.979
Al	5.302	5.267	5.272	5.280
Fe	16.065	16.083	16.546	16.231
Mn	0.729	0.627	0.625	0.660
Mg	5.373	5.462	5.219	5.351
Ca	7.653	7.684	7.681	7.673
Na	1.732	1.643	1.756	1.710
K	1.203	1.084	1.225	1.171
Cr				
Ba	0.198			
Ni	0.117			
O	40.231	40.017		40.124
TOTAL	99.375	98.490	98.866	98.910

Nd-38A

	1	2	3	4	5	Av.
Si	19.604	19.727	19.442	19.574	19.915	19.652
Ti	1.088	0.986	1.037	0.694	0.877	0.936
Al	6.814	6.772	6.851	6.843	6.403	6.737
Fe	12.239	12.341	12.791	13.040	13.279	12.738
Mn	0.163	0.153	0.243	0.187	0.301	0.209
Mg	6.724	6.632	6.382	6.557	6.614	6.582
Ca	8.575	8.533	8.477	8.359	8.554	8.500
Na	1.216	1.123	1.207	1.347	1.167	1.212
K	0.995	1.005	0.967	0.918	0.797	0.936
Cr		0.067				
Ba						
Ni						
O	41.151	41.134	40.873	40.948	41.196	41.060
TOTAL	98.569	98.475	98.269	98.466	99.094	98.575

K-content of hornblendes (cont.)

	Nd-49C						
	1	2	3	4	5	6	Av.
Si	19.333	19.680	18.959	19.273	19.328	19.346	19.320
Ti	1.296	1.020	1.090	1.387	1.101	1.118	1.169
Al	6.252	6.082	6.063	6.207	6.200	6.230	6.172
Fe	15.137	14.885	15.079	15.110	15.313	15.213	15.123
Mn	0.087		0.137		0.139	0.119	0.080
Mg	5.573	5.811	5.622	5.575	5.518	5.686	5.631
Ca	8.062	8.128	7.756	7.991	7.923	7.989	7.975
Na	1.504	1.390	1.342	1.403	1.467	1.548	1.442
K	1.088	0.978	0.901	1.023	1.106	1.088	1.031
Cr				0.061	0.064	0.068	
Ba					0.206		
Ni							
O	40.446	40.529	39.526	40.318	40.281	40.444	40.257
TOTAL	98.778	98.503	96.475	98.349	98.647	98.848	98.267

	Nd-107A			
	1	2	3	Av.
Si	19.639	19.286	19.179	19.368
Ti	0.797	0.814	0.822	0.811
Al	6.133	6.232	6.416	6.260
Fe	14.652	14.658	14.396	14.569
Mn	0.307	0.259	0.297	0.288
Mg	5.992	6.142	5.891	6.008
Ca	8.361	7.727	8.295	8.128
Na	1.461	1.298	1.459	1.406
K	1.361	1.291	1.348	1.333
Cr		0.068		
Ba	0.142			
Ni				
O	40.732	40.206	40.289	40.409
TOTAL	99.577	97.979	98.392	98.649